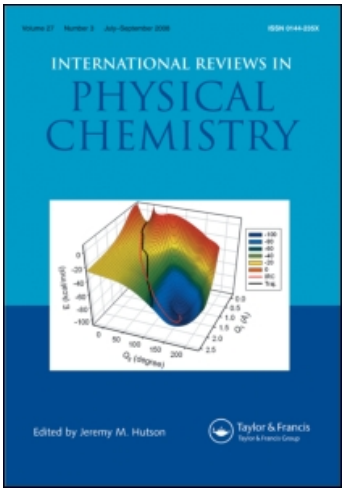

International Reviews in Physical Chemistry
Publication details, including instructions for authors and subscription information:
http://www.informaworld.com/smpp/title~content=t713724383

Femtosecond pump-probe spectroscopy: A theoretical analysis of transient signals and their relation to nuclear wave-packet motion

Niels E. Henriksen[a]; Volker Engel[b]
[a] Department of Chemistry, Technical University of Denmark, Lyngby, Denmark [b] Institut fur Physikalische Chemie, Universitat Wurzburg, Wurzburg, Germany

Online publication date: 26 November 2010

To cite this Article Henriksen, Niels E. and Engel, Volker(2001) 'Femtosecond pump-probe spectroscopy: A theoretical analysis of transient signals and their relation to nuclear wave-packet motion', International Reviews in Physical Chemistry, 20: 2, 93 — 126
To link to this Article: DOI: 10.1080/01442350010028523
URL: http://dx.doi.org/10.1080/01442350010028523

INT. REVIEWS IN PHYSICAL CHEMISTRY, 2001, VOL. 20, NO. 2, 93–126

Femtosecond pump–probe spectroscopy: a theoretical analysis of transient signals and their relation to nuclear wave-packet motion

NIELS E. HENRIKSEN

Department of Chemistry, Technical University of Denmark, DTU 207, DK-2800 Lyngby, Denmark

and VOLKER ENGEL†

Institut für Physikalische Chemie, Universität Würzburg, Am Hubland, D-97074 Würzburg, Germany

The first part of the review focuses on general expressions for pump–probe signals for the detection of processes such as intramolecular vibrational energy redistribution and unimolecular reaction dynamics. Analytical expressions are presented, which clearly display the connection between the time and the *average position* of the wave packet created by the pump pulse. We discuss how to obtain the highest resolution, that is how to obtain the closest correspondence between time and position. To that end we demonstrate, for example that the signal corresponding to a δ pump pulse can be recovered exactly from signals using pump pulses of finite temporal width. The second part is concerned with the relation between the transient signals and the *probability densities* associated with nuclear wave packets. Taking time-resolved photoelectron spectroscopy and pump–probe fluorescence spectroscopy as examples, we demonstrate that it is possible to obtain information about the temporal changes in probability densities as a function of interatomic distances. Finally, the phase-retrieval problem of quantum mechanics is discussed and it is shown that femtosecond time-resolved measurements in combination with other experimental techniques can provide sufficient information for the complete characterization of *wave packets* including the complex-valued phase.

Contents

† Email: voen@phys-chemie.uni-wuerzburg.de

International Reviews in Physical Chemistry ISSN 0144-235X print/ISSN 1366-591X online © 2001 Taylor & Francis Ltd
http://www.tandf.co.uk/journals
DOI: 10.1080/01442350010028523

1. Introduction

The dynamics of elementary physical and chemical processes can be followed in real time by femtosecond pump–probe spectroscopy [1–6].

In this review of the theoretical description of pump–probe signals, we focus on the detection of nuclear motion in gas-phase dynamics. That is, processes such as intramolecular vibrational energy redistribution (IVR) and unimolecular reaction dynamics are under investigation.

There are many important contributions to the theoretical description of pump–probe signals starting from the early days of femtochemistry [7–14], as well as many subsequent contributions [15–28]. For an extensive compilation of references see the chapter by J. Manz in [4].

Since we treat isolated molecules in the gas phase we shall employ a theoretical description in terms of wavefunctions and shall not discuss density matrix formulations which are better suited to the description of dynamics in condensed phases [29].

Various experimental techniques are employed to record time-resolved signals, for example transient absorption, four-wave mixing, ionization or Coulomb explosion spectroscopy; for reviews see for example [29–36]. Below we shall mainly concentrate on integrated pump–probe fluorescence spectroscopy and photoelectron spectroscopy.

In the first part of this review, we consider questions such as how the pump–probe signal should be interpreted and how the finite temporal width of the laser pulses affects the signal. As for the first question, we present, in the limit of ultrashort pump and probe pulses, analytical expressions for the pump–probe frequency-integrated fluorescence signal. Second, it is well known that the pump–probe signal can depend quite strongly on the parameters of the pump and probe laser (see for example [18]). An important question is therefore how to choose the optimal form of the laser pulses in order to obtain the most faithful detection of the underlying nuclear dynamics, that is the closest correspondence between the time and the average position of a localized wave packet.

In an ideal measurement, the pump pulse should launch a localized wave packet on a potential energy surface at a well defined time, that is create the closest possible correspondence to 'a rolling ball'. A δ pump pulse (i.e. a pulse which is short on a vibrational time scale but long on the electronic time scale) creates a Franck–Condon wave packet, that is a replica of the initial state times the transition dipole moment between the initial state and an electronically excited state, where this wave packet

subsequently evolves in time. The ideal δ pulse is not available in practice; therefore it is important to understand how, for example, a pump pulse with a finite temporal width affects the pump–probe signal. To that end, we shall show that it is, in fact, possible to eliminate the 'blurring' of the signal due to the finite duration of the pump pulse. Thus, one can always perform a deconvolution of the pump from the signal and obtain the signal corresponding to a δ pump pulse. Along this line, it is also important to consider how to choose an optimal probe pulse, again in order to obtain the closest correspondence between time and average position.

From the pump–probe signals, one can detect the dynamics of a wave packet as a function of time and directly extract various characteristic times, for example the time required to break a chemical bond [7] or characteristic vibrational periods [12]. Furthermore, one can even obtain a 'mapping of wave packets', that is information about coordinate-dependent probability changes, as will be discussed in the second part of the review.

This review is organized in the following way. Section 2 contains general expressions for pump–probe signals focusing on detection via frequency-integrated fluorescence. In section 3, the general expressions are applied in the derivation of analytical expressions for the pump–probe signal for the detection of transition states as well as asymptotic fragments in unimolecular reactions. In section 4, we demonstrate that the pump–probe signal can be expressed as a convolution of the pulse envelope with the signal corresponding to a δ pump pulse, if the signal for finite pump pulses is integrated over all pump frequencies. Thus, an exact deconvolution of the pump pulse is possible. The optimal choice of the probe pulse is also discussed. Section 5 establishes the connection between detected spectra and wave packets. After reviewing reflection principles known from frequency-resolved spectroscopy, similar mapping procedures are discussed in connection with femtosecond time-resolved spectroscopy. The review is concluded with a summary given in section 6.

2. Pump–probe signals

We consider, as illustrated in figure 1, the interaction between a molecule and two time-delayed pulses: a pump pulse and a probe pulse. Here we regard the field-induced coupling of different electronic states which are labelled as $|n\rangle$, where $n = 0, 1, 2$ respectively. Within the electric dipole approximation, the field–molecule coupling terms take the form (for absorption)

$$C_{\mathrm{pump}}(t) = -\mu_{10}\, a_1(t) \exp(-\mathrm{i}\omega_1 t), \qquad (1)$$
$$C_{\mathrm{probe}}(t) = -\mu_{21}\, a_2(t) \exp(-\mathrm{i}\omega_2 t)$$

where ω_1 and ω_2 are the carrier frequencies of the pump and probe pulses respectively, μ_{10} and μ_{21} are the projections of the transition dipole moments on the polarization vector of the electric field, and $a_1(t)$ and $a_2(t)$ are the pulse envelopes centred around $t = 0$ and the delay time $t = T$ respectively.

The pump pulse creates a wave packet which, according to first-order perturbation theory, can be written in the form

$$|\psi_1(t)\rangle = \frac{\mathrm{i}}{\hbar}\int_{-\infty}^{t} \exp\left(\frac{-\mathrm{i}(\hbar\omega_1 + \varepsilon_0)t'}{\hbar}\right) a_1(t') \exp\left(\frac{-\mathrm{i}\hat{H}_1(t-t')}{\hbar}\right) |\phi_0\rangle \,\mathrm{d}t', \qquad (2)$$

where

$$|\phi_0\rangle = \mu_{10}|\psi_0\rangle. \qquad (3)$$

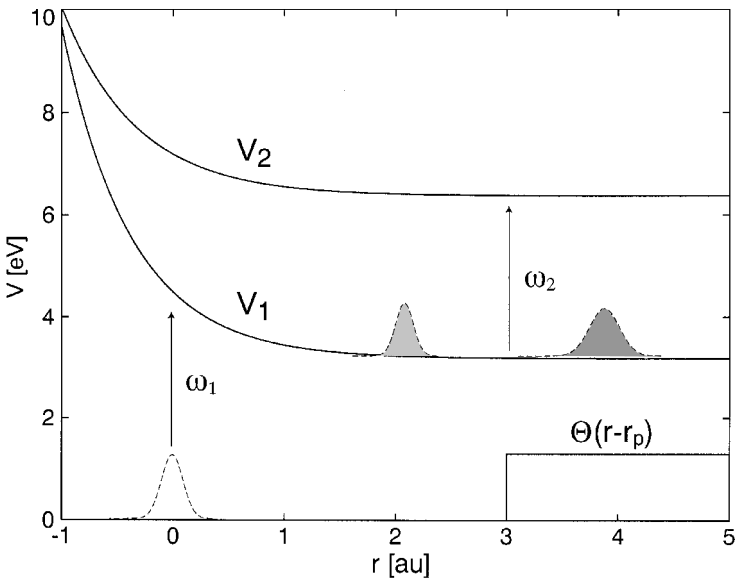

Figure 1. Pump–probe scheme for direct dissociation: the pump pulse (ω_1) prepares a wave packet in an excited electronic state with potential curve V_1. The probe pulse (ω_2) induces a transition to another electronic state (V_2) and the total fluorescence from this state is measured. The probe laser frequency is here chosen such that the wave packet is probed when it enters the asymptotic region where the distance r exceeds a critical distance r_p. This spatial window is denoted as $\Theta(r-r_p)$. The potentials represent a simple model for ICN dissociation where r is the I–C distance relative to the equilibrium position in the electronic ground state.

$|\psi_0\rangle$ is the initial stationary vibrational–rotational eigenstate of the molecule, before the arrival of the pump pulse, ε_0 is the energy of this state and $\hat{H}_1$ is the Hamiltonian for nuclear motion in electronic state (1). The lower limit in the integral has been extended from some finite time t_0, prior to the arrival of the pump pulse, to minus infinity using the fact that the pulse envelope $a_1(t)$ is effectively zero for times earlier than t_0. Equation (2) shows that the wave packet created by the pump pulse can be viewed as a superposition of Franck–Condon wave packets [37] given by

$$|M(t)\rangle = \exp\left(\frac{-i\hat{H}_1 t}{\hbar}\right)|\phi_0\rangle, \tag{4}$$

created over a period of time defined by the pulse envelope. It is a coherent superposition, however, which means that interference terms between Franck–Condon wave packets created at different times show up in the probability amplitude [38].

The probe pulse creates a new non-stationary state $|\psi_2(t)\rangle$. In the limit of non-overlapping pump and probe pulses, which we shall consider in the present paper, this state can be calculated according to first-order perturbation theory, now with $|\psi_1(t)\rangle$ as the initial state. At the final time, t_f, after the probe pulse has decayed to zero, it can be written in the form

$$|\psi_2(t_f)\rangle = \exp\left(\frac{-i\hat{H}_2(t_f - T)}{\hbar}\right)|\psi_2(T)\rangle, \tag{5}$$

where

$$|\psi_2(T)\rangle = \frac{\mathrm{i}}{\hbar}\int_{-\infty}^{\infty} \exp(-\mathrm{i}\omega_2 t)\, a_2(t) \exp\left(\frac{\mathrm{i}\hat{H}_2 t}{\hbar}\right) \mu_{21} \exp\left(\frac{-\mathrm{i}\hat{H}_1 t}{\hbar}\right) |\psi_1(T)\rangle \,\mathrm{d}t. \quad (6)$$

The total pump–probe fluorescence signal $P(T)$ is assumed to be proportional to the norm of $|\psi_2(t)\rangle$ after the probe pulse has decayed to zero:

$$P(T) = \langle \psi_2(t_\mathrm{f}) | \psi_2(t_\mathrm{f}) \rangle. \quad (7)$$

It depends on the form of the pump as well as the probe pulses, we have here only emphasized the dependence on the time delay T. The signal can be written in the form

$$P(T) = \langle \psi_1(T) | \hat{\mathscr{P}}_{12}(\omega_2) | \psi_1(T) \rangle, \quad (8)$$

where the probe operator

$$\hat{\mathscr{P}}_{12}(\omega_2) = \hat{P}\dagger(\omega_2)\, \hat{P}(\omega_2), \quad (9)$$

with

$$\hat{P}(\omega_2) = \frac{1}{\hbar}\int_{-\infty}^{\infty} \exp(-\mathrm{i}\omega_2 t)\, a_2(t) \exp\left(\frac{\mathrm{i}\hat{H}_2 t}{\hbar}\right) \mu_{21} \exp\left(\frac{-\mathrm{i}\hat{H}_1 t}{\hbar}\right) \mathrm{d}t; \quad (10)$$

this expression incorporates the possible motion of the wave packet, $|\psi_1(t)\rangle$, during the action of the probe pulse.

For an ultrashort probe pulse, that is $a_2(t)$ is strongly peaked around $t = T$, one can introduce the following approximation [9, 19–21, 24–26, 39]

$$\exp\left(\frac{\mathrm{i}\hat{H}_2 t}{\hbar}\right) \exp\left(\frac{-\mathrm{i}\hat{H}_1 t}{\hbar}\right) = \exp\left(\frac{\mathrm{i}(V_2 - V_1) t}{\hbar}\right). \quad (11)$$

This approximation implies that only terms linear in time are retained, since

$$\exp(\hat{A}) \exp(\hat{B}) = \exp(\hat{C}), \quad (12)$$

where $\hat{C} = \hat{A} + \hat{B} + [\hat{A}, \hat{B}]/2 + \cdots$. That is, one neglects commutators between the kinetic energy operator and the coordinate-dependent terms in the integral, that is potentials and the transition dipole moment. The signal can now be written in the form

$$\begin{aligned} P(T) &= \int \psi_1^*(\mathbf{q}, T)\, |F[D(\mathbf{q}) - \omega_2]|^2 \psi_1(\mathbf{q}, T)\, \mathrm{d}\mathbf{q} \\ &= \int |F[D(\mathbf{q}) - \omega_2]|^2 |\psi_1(\mathbf{q}, T)|^2\, \mathrm{d}\mathbf{q}, \end{aligned} \quad (13)$$

where

$$F[D(\mathbf{q}) - \omega_2] = \mu_{21} \int_{-\infty}^{+\infty} a_2(t) \exp\left(\frac{\mathrm{i}(D(\mathbf{q}) - \hbar\omega_2) t}{\hbar}\right) \mathrm{d}t. \quad (14)$$

Here $\mathbf{q}$ denotes the collection of all nuclear coordinates, and $D(\mathbf{q}) = V_2(\mathbf{q}) - V_1(\mathbf{q})$ is the difference between the potential energy surfaces in the electronic states (2) and (1). Thus, the signal measures the norm of the wave packet ψ_1 at time T within the window $|F[D(\mathbf{q}) - \omega_2]|^2$ (Franck–Condon window).

The expressions presented above are valid for direct as well as indirect ('standard') unimolecular reactions. The relation between pump–probe signals and the kinetics of indirect unimolecular reactions, that is the exponential decay of reactants and the

exponential rise of the product population, has been highlighted recently [40]. To that end, a description where the wave-packet dynamics is expressed in terms of the decay of quasibound resonance states was invoked.

Consider, as an example, a Gaussian probe pulse $a_2(t) = (\gamma/\pi)^{1/2}\exp[-\gamma(t-T)^2]$. The probe operator (Franck–Condon window) takes the form

$$|F[D(\mathbf{q})-\omega_2]|^2 = |\mu_{21}|^2 \exp\left(\frac{-[\omega_2 - D(\mathbf{q})/\hbar]^2}{2\gamma}\right). \tag{15}$$

In order to enhance insight, we limit now the discussion to one degree of freedom, replacing the vector $\mathbf{q}$ by the coordinate r.

It is interesting to note that (neglecting the coordinate dependence of the transition dipole moment) the correction to equation (11) in the order t^2 contains the commutator

$$[\hat{T}, D] = -\frac{\hbar^2}{2m}\left(\frac{\mathrm{d}^2 D}{\mathrm{d}r^2} + 2\frac{\mathrm{d}D}{\mathrm{d}r}\frac{\mathrm{d}}{\mathrm{d}r}\right), \tag{16}$$

where $\hat{T}$ denotes the kinetic energy operator and m the mass. Assuming a linear difference potential, we recognize that the commutator is proportional to the momentum operator. As a consequence, an incorporation of the correction term accounts for the motion of the wave packet during the excitation process. If now the momentum operator is replaced by its expectation value $\langle p\rangle_T$, calculated with the state $|\psi_1(T)\rangle$, the correction term to second order in t is of the form

$$\exp\left(-\frac{1}{2}\frac{[\hat{T}, D]t^2}{\hbar^2}\right) = \exp\left(\mathrm{i}\frac{1}{2}\frac{\mathrm{d}D}{\mathrm{d}r}\frac{\langle p\rangle_T}{m}\frac{t^2}{\hbar}\right). \tag{17}$$

Note that this phase factor exclusively depends on time. In the case when a linearly chirped probe pulse with a time-dependent frequency $\omega_2(t) = \omega_2 + \alpha t$ is employed, the chirp parameter α may be chosen as $\alpha = -\frac{1}{2}(\mathrm{d}D/\mathrm{d}r)[\langle p\rangle_T/(m/\hbar)]$ so that the term (17) is, within the employed approximations, exactly cancelled. This allows, by adjusting the chirp parameter, inward and outward motion of vibrational wave packets to be distinguished, as was documented by use of time-resolved photoelectron spectroscopy [41].

2.1. *Detection of transition states*

We consider first the detection of transition states, that is configurations between reactants and products in unimolecular reactions. The detection of transient configurations corresponding to IVR or simple vibrational motion in a diatomic molecule is also within the framework of the following discussion.

We linearize the difference potential around the 'Franck–Condon point', where $\hbar\omega_2 = D(r_\mathrm{p})$. Thus,

$$D(r) = D(r_\mathrm{p}) + g(r - r_\mathrm{p}), \tag{18}$$

where $g = D'_{r=r_\mathrm{p}}$ is the derivative of the difference potential. We have assumed that the equation $\hbar\omega_2 = D(r_\mathrm{p})$ has only one solution for r_p but it should be noted that, in some cases, the equation can have more than one solution. Equation (15) now takes the form

$$|F[D(r)-\omega_2]|^2 = |\mu_{21}|^2 \exp\left[-\left(\frac{g}{\hbar}\right)^2 \frac{(r-r_\mathrm{p})^2}{2\gamma}\right]. \tag{19}$$

Thus, the probe operator is a Gaussian around the Franck–Condon point $r = r_\mathrm{p}$. The position of this point depends on the probe frequency ω_2. If the probe pulse is too short

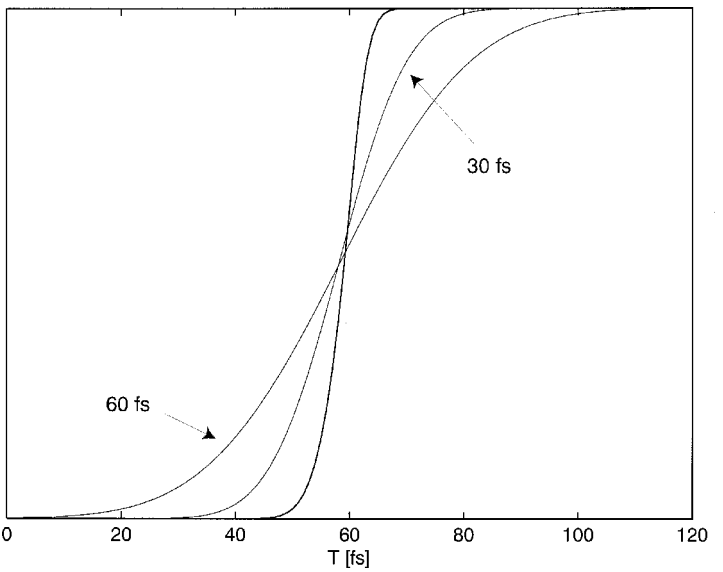

Figure 2. Pump–probe signal for a δ pump pulse (——) and for 30 and 60 fs Gaussian pump pulses (full width at half-maximum). All signals were normalized to the same asymptotic value. The zero of time is chosen such that it is at the centre of the pump pulse.

($\gamma \to \infty$) or, equivalently, $g \to 0$, the probing becomes insensitive to the potential energy difference. In this limit where the window is, essentially, constant over the width of the wave packet (at all times), $P(T) \to |\mu_{21}|^2 \int \mathrm{d}r\, |\psi_1(r, T)|^2$, where the coordinate dependence of the transition dipole moment is neglected as in the derivation of equation (13). Thus, in this limit, the signal is proportional to the norm of the wave packet and, consequently, independent of the position.

2.2. *Detection of fragments in unimolecular reactions*

In the case of fragment detection for a dissociation process, the carrier frequency of the probe laser matches the asymptotic value of the difference potential. The approximation in equation (18) is not appropriate in this case. Instead, we write

$$D(r) = \begin{cases} D(r_\mathrm{p}) & \text{for } r \geqslant r_\mathrm{p}, \\ D(r_\mathrm{p}) + g(r - r_\mathrm{p}) & \text{for } r < r_\mathrm{p}, \end{cases} \tag{20}$$

which implies that the probe state is equivalent to equation (19) for $r < r_\mathrm{p}$ and constant for $r \geqslant r_\mathrm{p}$. If the probe pulse is not too short or, equivalently, $g \to \infty$, the probe operator is approximately given by the form

$$|F[D(r) - \omega_2]|^2 = |\mu_{21}|^2 \Theta(r - r_\mathrm{p}), \tag{21}$$

that is a step function.

The dissociation of ICN into I+CN is chosen as a numerical example (see figure 1). In the first gas-phase femtosecond time-resolved experiments, Zewail and co-workers [42, 43] investigated this system. Quantum calculations were performed within an one-dimensional model by Williams and Imre [8]; see [44] for details. Figure 2 shows pump–probe signals for a δ pump pulse (solid curve) and for 30 and 60 fs Gaussian pump pulses (full width at half-maximum) with a detection window as in equation (21), which starts at $r_\mathrm{p} = 3$ au. In the plot, the zero of time is chosen such that it is at the maximum of the envelope function for the respective pump pulses. The

broadening of the signal due to finite pulse widths is clearly seen in the figure. In addition, it is observed that the three curves cross almost at the same point close to a time of 60 fs. It should, however, be noted that a symmetric Gaussian pump pulse was used and similar agreement would not have been obtained with an asymmetric pump pulse. Furthermore, the frequency of the 30 and 60 fs pump pulses was chosen to be at the maximum of the absorption based (4.5 eV), and one should keep in mind that, in general, the signals will be frequency dependent.

3. Analytical expressions for the pump–probe signal

The first analytical expression for pump–probe signals was presented by Bersohn and Zewail [7]. Their expression was given heuristically and based on a classical description of the nuclear dynamics.

In this section, we shall show that in the limit of an ultrashort pump (and probe) pulse the general form of the pump–probe signal can be obtained analytically.

3.1. *The pump excitation*

We write equation (2) in the form

$$|\psi_1(t)\rangle = \frac{\mathrm{i}}{\hbar}\exp\left(\frac{-\mathrm{i}\hat{H}_1 t}{\hbar}\right)\int_{-\infty}^{t} \mathrm{d}t' \exp\left(\frac{-\mathrm{i}(\hbar\omega_1+\varepsilon_0)t'}{\hbar}\right) a_1(t')\exp\left(\frac{\mathrm{i}\hat{H}_1 t'}{\hbar}\right)|\phi_0\rangle. \quad (22)$$

The pulse envlope of the pump is centred at the time $t = 0$ and represented by a Gaussian form

$$a_1(t) = E_0\left(\frac{\gamma}{\pi}\right)^{1/2}\exp(-\gamma t^2), \quad (23)$$

where γ is large, corresponding to an ultrashort pump pulse. For such a pulse, we can again use equation (12) to split the time evolution operator into two parts, one which depends on the potential V_1 and one which depends on the kinetic energy operator $\hat{T}$. Equation (22) can now be written in the form

$$|\psi_1(t)\rangle = \frac{\mathrm{i}}{\hbar}\exp\left(-\frac{\mathrm{i}\hat{H}_1 t}{\hbar}\right)\int_{-\infty}^{t} \mathrm{d}t' \exp\left(\frac{-\mathrm{i}[\hbar\omega_1-(V_1-\varepsilon_0)]}{\hbar}\right) a_1(t')\exp\left(\frac{\mathrm{i}\hat{T}t'}{\hbar}\right)|\phi_0\rangle. \quad (24)$$

The propagation involving the kinetic energy operator corresponds to the propagation of the initial state as a free particle. Thus, in the present case, this propagation reflects the spreading of the initial state during the interaction with the ultrashort pump pulse. In the following, we neglect this spreading. For times $t > 0$, such that the magnitude of the envelope function of the pump pulse is negligible, the integral (note the similarity with the Franck–Condon window in equation (14)) corresponds to a Fourier transform of the pulse envelope, and

$$|\psi_1(t)\rangle = \frac{-\mathrm{i}E_0}{\hbar}\exp\left(\frac{-\mathrm{i}\hat{H}_1 t}{\hbar}\right)|\phi_0\rangle\exp\left(\frac{-\Omega^2}{4\gamma}\right), \quad (25)$$

where $\Omega = \omega_1-(V_1-\varepsilon_0)/\hbar$.

A one-dimensional model is considered and, for a molecule in the vibrational ground state, $\phi_0(r)$ is approximately a Gaussian, that is

$$\phi_0(r) = \exp\left(\frac{\mathrm{i}}{\hbar}[A_0(r-r_0)^2+s_0]\right), \quad (26)$$

where $A_0 = \mathrm{i}\,\mathrm{Im}(A_0) = \mathrm{i}m\omega/2$, ω is the vibrational frequency, m is the mass, and normalization implies that $s_0 = (\mathrm{i}\hbar/4)\ln\{\pi\hbar/[2\,\mathrm{Im}\,(A_0)]\}$. Next, in the Fourier transform of the pulse envelope, we linearize the potential around the centre of the initial state,

$$V_1(r) = V_1(r_0) + \alpha(r - r_0), \tag{27}$$

where α is the derivative of the potential at $r = r_0$.

After substitution of equations (26) and (27) into equation (25), the wave packet created by the pump pulse can be written in the form

$$|\psi_1(t)\rangle = \frac{\mathrm{i}E_0}{\hbar}\exp\left(\frac{-\mathrm{i}\hat{H}_1 t}{\hbar}\right)|\Phi_0\rangle, t > 0 \tag{28}$$

where

$$\langle r\,|\,\Phi_0\rangle = \exp\left(\frac{-m\omega(r-r_0)^2}{2\hbar} + \frac{\mathrm{i}s_0}{\hbar}\right) \times \exp\left(\frac{-\alpha^2(r-r_0-r_\mathrm{e})^2}{4\hbar^2\gamma}\right), \tag{29}$$

and $r_\mathrm{e} = \{\hbar\omega_1 - [V_1(r_0) - \varepsilon_0]\}/\alpha$. Thus, the wavefunction is a product of two Gaussians, the initial Gaussian, that is the Gaussian generated by a δ pump pulse, times a displaced Gaussian where the displacement is proportional to the detuning $\hbar\omega_1 - V_1(r_0)$. The norm of this wave packet created by an ultrashort pump pulse depends on the detuning. Thus, a large detuning implies that the norm eventually vanishes. The product of the two Gaussians is proportional to a single Gaussian centred at a position given as a weighted sum of r_0 and r_e. For an alternative derivation of the same result, see [44] (for a similar expression, see also [9]).

For $\hbar\omega_1 = V_1(r_0) - \varepsilon_0$, that is 'on-resonant' pumping at the centre of the absorption band, $\langle r\,|\,\Phi_0\rangle$ takes the Gaussian form

$$\langle r\,|\,\Phi_0\rangle = \exp\left[-\left(\frac{m\omega}{2\hbar} + \frac{\alpha^2}{4\hbar^2\gamma}\right)(r-r_0)^2 + \frac{\mathrm{i}s_0}{\hbar}\right], \tag{30}$$

with the same expectation value of the position as in the initial state in equation (26), that is r_0. The width of the wave packet has also changed from $\hbar/2m\omega$ to $(\Delta r)_0^2 = \hbar/(2m\omega + \alpha^2/\hbar\gamma)$, that is the width is reduced compared with the Franck–Condon wave packet. Since the Gaussian is still a minimum uncertainty packet, the reduced width implies that an ultrashort pulse as defined above, produces a squeezed state. Similar squeezing phenomena have been discussed previously [45, 46]. In the limit where $\gamma \to \infty$, corresponding to a δ pump pulse, equation (29) reduces, as expected, to the Franck–Condon wave packet.

We consider in the following 'on-resonant' pumping where $r_\mathrm{e} = 0$ in equation (29) corresponding to the initial state in equation (30), and assume that the dynamics can be described within a (time-dependent) local harmonic approximation to the potential. Then $\langle r\,|\,\psi_1(t)\rangle$ in equation (28) can at all times be represented by a Gaussian wave packet of the form [47, 48]

$$\langle r\,|\,G(t)\rangle = \exp\left(\frac{\mathrm{i}}{\hbar}[A_t(r-r_t)^2 + p_t(r-r_t) + s_t]\right). \tag{31}$$

The time evolution of the parameters is given by simple equations of motion. For example, the centre of the wave packet (r_t, p_t) evolves in time according to Hamilton's equations of motion.

3.2. *Detection of transition states*

For detection of transition states, using equations (13) and (19), and also equations (28) and (29) (for $r_e = 0$) the pump–probe signal takes the form

$$P(T) = \frac{E_0^2|\mu_{21}|^2}{\hbar^2[2\pi(\Delta r)_T^2]^{1/2}}\int_{-\infty}^{\infty} \mathrm{d}r \exp\left[-\left(\frac{g}{\hbar}\right)^2\frac{(r-r_p)^2}{2\gamma}\right]\exp\left(-\frac{(r-r_T)^2}{2(\Delta r)_T^2}\right)$$
$$= \frac{E_0^2|\mu_{21}|^2}{\hbar^2}\left(\frac{2\gamma}{2(\Delta r)_T^2(g/\hbar)^2+2\gamma}\right)^{1/2}\exp\left(-\frac{(g/\hbar)^2}{2(\Delta r)_T^2(g/\hbar)^2+2\gamma}(r_T-r_p)^2\right), \quad (32)$$

where r_T and $(\Delta r)_T$ are the expectation value and uncertainty respectively of the position at time T. Thus, the signal takes a Gaussian form as the wave packet moves in and out of the probe window (under the assumption of no spreading and constant velocity as the Gaussian wave packet crosses the window). The width of the signal is related to the width of the wave packet and to the duration of the probe pulse. Thus, a short probe (γ large) or a wave packet with a large uncertainty in the position gives a broad signal. Equation (32) also shows that the pre-exponential factor in the expression will decay as the wave packet spreads. That is, if the wave packet can pass repeatedly through the probe window, the peak height of the signal will decay when the wave packet spreads.

3.3. *Detection of fragments in unimolecular reactions*

We consider now fragment detection for a dissociation process, where the carrier frequency of the probe laser matches the asymptotic value of the difference potential. To a good approximation, the detection window can be represented by the expression in equation (21). Thus, the pump–probe signal becomes, according to equation (13),

$$P(T) = |\mu_{21}|^2\int_{r_p}^{\infty} \mathrm{d}r\,|\psi_1(r,T)|^2. \quad (33)$$

Using again the Gaussian wave packet approximation, the integral takes the form [37]

$$P(T) = \frac{E_0^2|\mu_{21}|^2}{\hbar^2(2\pi(\Delta r)_T^2)^{1/2}}\int_{r_p}^{\infty} \mathrm{d}r \exp\left(-\frac{(r-r_T)^2}{2(\Delta r)_T^2}\right), \quad (34)$$

which can be expressed as

$$P(T) = \frac{E_0^2|\mu_{21}|^2}{2\hbar^2}\left[1+\mathrm{erf}\left(\frac{r_T-r_p}{2^{1/2}(\Delta r)_T}\right)\right], \quad (35)$$

where the error function is defined by

$$\mathrm{erf}(x) = \frac{2}{\pi^{1/2}}\int_0^x \exp(-u^2)\,\mathrm{d}u. \quad (36)$$

We observe that, at the time when the centre of the wave packet has reached the detection window, that is $r_T = r_p$, $P(T)$ is at half of its asymptotic value. It should also be noted that the time derivative of the signal at this point is given by the ratio of the

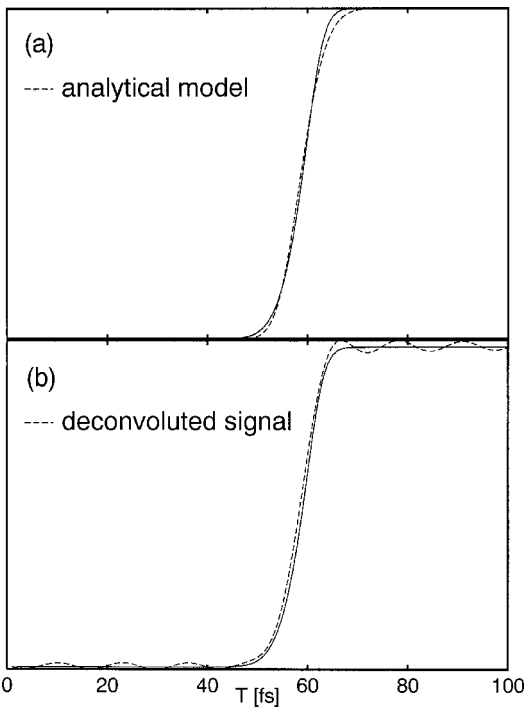

Figure 3. (*a*) The result of the analytical model compared with the numerically calculated pump–probe signal for a δ pump pulse (——). (*b*) The pump–probe signal deconvoluted from a signal obtained with a 30 fs (full width at half-maximum) Gaussian pump pulse centred at t_p = 60 fs. The pump–probe signal for a δ pump pulse is also shown (——).

mean speed to the uncertainty $(\Delta r)_T$ [37]. This ratio gives the intrinsic time resolution according to quantum mechanics. In the limit where the uncertainty is negligible, the signal approaches a step function, as expected from a classical mechanical description of the dissociation dynamics.

Figure 3 (*a*) shows the almost exact agreement between the pump–probe signal for a δ pump pulse (solid curve) obtained by numerical solution of the Schrödinger equation, and the result obtained from the analytical expression in equation (35). As pointed out above, the slope of the signal depends on the width of the wave packet and, consequently, the spreading of the wave packet as it travels from the initial position into the detection window. The excellent agreement shows that the time-dependent local harmonic approximation to the exponential potential is well fulfilled in the present case.

The analytical model presented above documents that the initial values of the Gaussian wave-packet parameters depend on the form of the pump laser (see equation (30)). In addition, a broad initial state will tend to give a 'broad' signal (i.e. a small slope). We can also understand, at least qualitatively, how a change in the frequency of the pump can change the 'dissociation time', that is the time when the centre of the wave packet has reached the detection window. From equation (29), with a repulsive potential (α negative) as in figure 1, we can understand how the wave packet created by the pump pulse changes as a function of the frequency. With 'off-resonant' frequencies at the wings of the absorption band, that is $\hbar\omega_1 > V_1(r_0)$ and $\hbar\omega_1 < V_1(r_0)$, the maximum in the amplitude of the wave packet will be displaced to $r < r_0$ and

$r > r_0$ respectively. Compared with the pumping at the centre of the absorption band, the final average momentum will accordingly be higher when $\hbar\omega_1 > V_1(r_0)$ and lower when $\hbar\omega_1 < V_1(r_0)$. Thus, a shorter dissociation time is expected in the first case whereas, when $\hbar\omega_1 < V_1(r_0)$, the dissociation time is expected to be longer than in the on-resonant case described by equation (35).

Leaving the ultrashort pump–probe limit assumed in equation (30), a pump pulse with a long duration will create a broad wave packet. Assuming that this wave packet can be represented by a Gaussian wave packet, equation (35) shows that a wave packet with a large uncertainty in the position gives a broad signal, in accordance with the numerical simulations in figure 2.

4. Optimal laser pulses

The signal $P(T)$ gives, essentially, the connection between the delay time and the average position of the wave packet measured within the Franck–Condon window. We have seen that the duration of the laser pulses affects the form of the signal. Thus, the signal is broadened when the duration of the pump pulse is increased. For the probing, an ultrashort probe pulse is, however, not an optimal pulse since such a pulse gives a signal where the connection between the delay time and the average position is 'blurred'. We consider now how to choose the optimal form of the laser pulses in order to obtain the closest correspondence between time and average position, that is how to minimize the width of the signal. For the pump pulse, we shall show that the signal corresponding to the optimal pump can be extracted from the experimental signal whenever the pulse envelope is known.

4.1. *The deconvolution of the pump pulse*

It is often assumed that the combined effect of two contributions to an experimental signal can be expressed as a convolution of the individual contributions [49]. Specifically, in the field of pump–probe spectroscopy, it has been suggested [50] that, for a pump pulse with finite width, the pump–probe signal can be analysed in the following way: the signal has a certain time dependence $S_{FC}(t)$ for an infinitely narrow δ pump pulse. When the pump pulse has a finite width, its intensity has a time dependence given by $I(t)$, and now each molecule is transferred to the excited state at a slightly different time t'. The resulting signal at time t is a sum of terms of the form $I(t')\,S_{FC}(t-t')$. This sum (integral) takes the form of a convolution of the intensity $I(t)$ with the δ pulse signal $S_{FC}(t)$. We consider now the validity of such an approach within the framework of quantum mechanics.

In what follows, we shall show that it is possible to extract the signal for a Franck–Condon wave packet from measurements using pump pulses of finite temporal width [44]. We start with the general expression for pump–probe signals in the limit of non-overlapping pump and probe pulses, and write equation (8) in the form

$$P(\omega_1, T) = \langle \psi_1(T) \,|\hat{\mathscr{P}}_{12}(\omega_2)\,|\psi_1(T)\rangle, \tag{37}$$

where $\hat{\mathscr{P}}_{12}(\omega_2)$ is defined in equation (9).

Now using the first-order expression in equation (2) for the wave packet,

$$P(\omega_1, T) = \frac{1}{\hbar^2}\int_{-\infty}^{T} \mathrm{d}t'' \int_{-\infty}^{T} \mathrm{d}t' \exp\left[\mathrm{i}\omega_1(t''-t')\right] a_1(t')\,a_1(t'') \times \langle M(T-t'')|\hat{\mathscr{P}}_{12}(\omega_2)|M(T-t')\rangle, \tag{38}$$

where

$$|M(T-t)\rangle = \exp\left(\frac{-\mathrm{i}\hat{H}_1(T-t)}{\hbar}\right)|\phi_0\rangle \tag{39}$$

is the Franck–Condon wave packet associated with a δ pump pulse excitation. This expression shows that, at a given pump frequency, quantum-mechanical interference terms show up between Franck–Condon wave packets created at different times. Furthermore, these 'off-diagonal' terms are frequency dependent.

We integrate now over the frequencies of the pump laser. The signal $S(T)$ can then be written as

$$\begin{aligned} S(T) &= \int_{-\infty}^{\infty} P(\omega_1, T)\,\mathrm{d}\omega_1 \\ &= \frac{\pi}{2\hbar^2}\int_{-\infty}^{T}\mathrm{d}t''\int_{-\infty}^{T}\mathrm{d}t'\,\delta(t''-t')a_1(t')a_1(t'')\langle M(T-t'')|\hat{\mathscr{P}}_{12}(\omega_2)|M(T-t')\rangle \\ &= \frac{\pi}{2\hbar^2}\int_{-\infty}^{T}\mathrm{d}t'\,[a_1(t')]^2\langle M(T-t')|\hat{\mathscr{P}}_{12}(\omega_2)|M(T-t')\rangle. \end{aligned} \tag{40}$$

This is an integral of signals for Franck–Condon wave packets created at different times with amplitudes given by the square of the pulse envelope. $P(\omega_1, T)$ is only non-zero within the absorption band of electronic state (1), therefore the integration over frequency can be extended to infinity.

This expression can be rewritten as a convolution

$$\begin{aligned} S(T) &= \frac{\pi}{2\hbar^2}\int_{-\infty}^{T}\mathrm{d}t'\,[a_1(t')]^2\langle M(T-t')|\hat{\mathscr{P}}_{12}(\omega_2)|M(T-t')\rangle \\ &= \frac{\pi}{2\hbar^2}\int_{0}^{\infty}\mathrm{d}y\,[a_1(T-y)]^2\langle M(y)|\hat{\mathscr{P}}_{12}(\omega_2)|M(y)\rangle \\ &= \frac{\pi}{2\hbar^2}\int_{-\infty}^{\infty}\mathrm{d}y\,[a_1(T-y)]^2\Theta(y)\langle M(y)|\hat{\mathscr{P}}_{12}(\omega_2)|M(y)\rangle, \end{aligned} \tag{41}$$

where we changed variable to $y = T-t'$ in the second line. In the last line the lower integration limit is extended to minus infinity, using the fact that $a_1(T-y)$ has its maximum for $y = T$ and $a_1(T-y) \approx 0$ for $y \leqslant 0$ since the duration is substantially smaller than the delay time T (the basic assumption of non-overlapping pump and probe pulses). Thus, the frequency-integrated signal is expressed as a convolution between the square of the pulse envelope and the signal for a Franck–Condon wave packet:

$$S_{\mathrm{FC}}(t) = \Theta(t)\langle M(t)|\hat{\mathscr{P}}_{12}(\omega_2)|M(t)\rangle. \tag{42}$$

In order to obtain the frequency-integrated signal experimentally, it is necessary to make a series of measurements covering the entire absorption band.

The deconvolution of the pump pulse is, in principle, straightforward using some basic rules of the Fourier transformation [49]. Thus, the Fourier transform of a convolution is equal to the product of the Fourier transforms of each function. This product can then simply be divided by the Fourier transform of the squared pulse envelope, in order to isolate the desired signal for the Franck–Condon wave packet. Details can be found in [44].

Thus, in short, the total (integrated) pump–probe fluorescence signal can be expressed as a convolution between the square of the pulse envelope and the signal for

a Franck–Condon wave packet. This is an exact statement when the signal is integrated over the frequency of the pump laser, that is over the entire absorption band. The derivation was based on first-order perturbation theory for the field–molecule coupling and, furthermore, it was assumed that the pump and probe pulses are non-overlapping. When the signal is expressed as a convolution it is possible to eliminate the 'blurring' due to the finite duration of the pump pulse. Thus, an exact procedure has been established for the extraction of the signal for a Franck–Condon wave packet from measurements using a pump pulse of finite temporal width.

Figure 3(*b*) shows the pump–probe signal for a δ pump pulse (solid curve) and the result obtained by deconvolution from a frequency-integrated signal (equation (40)) calculated with a 30 fs (full width at half-maximum) Gaussian pump pulse centred at t_p = 60 fs. The agreement is perfect and within the numerical resolution of the calculation. The small oscillations in the deconvoluted signal come from small absolute values (beyond the numerical accuracy) in the Fourier transform of the convoluted signal (41) [44]. It should be noted that, essentially, the same good agreement is obtained from a deconvolution, and not from the frequency-integrated signal but from a signal corresponding to a pump frequency at the maximum of the absorption spectrum. The absorption band for ICN is fairly narrow and symmetric and, in fact, a deconvolution at any pump frequency within this band will give a result which is fairly close to the signal given in figure 3.

4.2. *The optimal probe pulse*

The signal (as the wave packet moves in and out of the probe window) depends on the temporal width of the probe pulse (equation (32)). A δ probe pulse (i.e. a pulse which is short on the time scale of vibrational motion but long on the electronic time scale) is not the optimal pulse for the detection of nuclear motion, since such a pulse gives absorption at all internuclear positions. The width of the signal decreases as the temporal width of the probe pulse is increased. The derivation of equation (32) was, however, based on the assumption of an ultrashort probe pulse. Consequently we cannot determine an optimal temporal width based on this expression. When equation (11) is replaced by a relation which is valid to second order in time, with a short Gaussian probe pulse with a temporal width t_p, it is again possible to derive an analytical expression [25]. This expression includes, approximately, the motion of the wave packet during probing. It can be shown that the highest resolution of the signal is obtained when [25]

$$t_p = \frac{1}{(g v_c)^{1/2}} \tag{43}$$

where g is defined in equation (18), that is it is the slope of the difference potential at the Franck–Condon point, and v_c is the expectation value of the velocity. Thus, a short probe is required when the velocity and/or slope is large. The optimal probe pulse must, however, normally be found experimentally, since the velocity of the wave packet as well as the slope of the difference potential are unknown.

5. Mapping of molecular wave packets

In the preceding sections we discussed the relation of femtosecond time-resolved pump–probe signals to the nuclear wave-packet motion and in particular the influence of the characteristics of pump and probe laser pulses. The issue was to show how far these signals reflect properties of the quantum dynamics prepared by femtosecond

excitation. In the second part of this review we shall ask a more ambitious question: is it possible to characterize temporal changes in the coordinate-dependent probability density distribution within a time-resolved measurement? Alternatively, an even more ambitious question: can such measurements provide us with the knowledge about the complex-valued wavefunction describing a molecular ensemble?

To connect to common grounds we shall first review *reflection principles* which are well known in continuous-wave spectroscopy measurements [51, 52]. As examples we consider molecular photodisociation and atomic ionization. Similar principles can also be found in continuum resonance Raman [53–57] or state-selected photofragment spectroscopy [58, 59]. After this discussion we turn to femtosecond transient experiments to illustrate that indeed, at least for simple systems, the probability-density distribution and its temporal changes can directly be monitored using various pump–probe arrangements. Finally, we discuss the *phase retrieval problem* of quantum mechanics and show that it is possible to characterize the wavefunction of a system completely with the help of femtosecond spectroscopy.

5.1. *Reflection principles of continuous-wave spectroscopy*

5.1.1. *Molecular bound-to-free transitions*

As a first example we treat the bound-to-free transition in a diatomic molecule, as illustrated in figure 1, that is a photodissociation process. The absorption spectrum is given by the 'golden rule' expression [60]

$$\sigma(\omega_1) \sim \sum_f |\langle \psi_f - |\mu_{10}|\psi_0\rangle|^2 \delta(E_f - (\varepsilon_0 + \omega_1)) \tag{44}$$

Here $|\psi_0\rangle$ denotes the initial bound state of energy ε_0, $|\psi_f - \rangle$ the scattering state of energy E_f, ω_1 is the photon energy and μ_{10} is the transition dipole moment between the electronic states $|0\rangle$ and $|1\rangle$.

Recasting equation (44) in a time-dependent form [61–63] yields

$$\sigma(\omega_1) \sim \int \exp(\mathrm{i}\omega_1 t)\, c(t)\, \mathrm{d}t, \tag{45}$$

with the time correlation function $c(t)$ defined as

$$c(t) = \left\langle \mu_{10}\psi_0 | \exp\left(\frac{-\mathrm{i}\hat{H}_1 t}{\hbar}\right) \mu_{10} \exp\left(\frac{\mathrm{i}\hat{H}_0 t}{\hbar}\right) \psi_0 \right\rangle. \tag{46}$$

A reflection principle is now derived using an approximation as introduced in section 2 (equation (11)), namely

$$\exp\left(\frac{-\mathrm{i}\hat{H}_1 t}{\hbar}\right) \mu_{10} \exp\left(\frac{\mathrm{i}\hat{H}_0 t}{\hbar}\right) \sim \exp\left(\frac{-\mathrm{i}V_1 t}{\hbar}\right) \mu_{10} \exp\left(\frac{\mathrm{i}V_0 t}{\hbar}\right) = \exp\left(\frac{-\mathrm{i}Dt}{\hbar}\right) \mu_{10}, \tag{47}$$

where $D = V_1 - V_0$ is a difference potential which, in our case, depends on the interatomic distance r of the diatomic molecule. The spectrum then takes the form

$$\sigma(\omega_1) \sim \iint |\mu_{10}\psi_0(r)|^2 \exp\left[\mathrm{i}\left(\omega_1 - \frac{D(r)}{\hbar}\right) t\right] \mathrm{d}t\, \mathrm{d}r. \tag{48}$$

The time integral is a representation of the δ function (apart from unimportant factors) so that, using its properties [60], the spectrum can be expressed as

$$\sigma(\omega_1) \sim \sum_i \frac{1}{|D'(r_i)|} |\mu_{10}\psi_0(r_i)|^2. \tag{49}$$

Here the points r_i are roots of the equation

$$D(r_i) - \omega_1 = 0. \tag{50}$$

It is instructive to evaluate the spectrum for the case of a linear difference potential (equation (18)), when only a single solution r_1 of equation (50) exists:

$$\sigma(\omega_1) \sim \frac{1}{|g|} |\mu_{10}\psi_0(r_1)|^2. \tag{51}$$

We now recognize that the absorption spectrum at a fixed photon energy ω_1 is proportional to the product function $|\mu_{10}(\rho_1)\psi_0(r_1)|^2$ at the distance r_1 where the difference potential equals ω_1, that is where equation (50) holds. In particular, if the r dependence of the dipole moment function is neglected (Condon approximation), the absorption spectrum reflects the modulus squared of the initial vibrational wavefunction. Many examples have been found which show the above derived reflection principle to be valid; for an extended discussion see for example the book by Schinke [64].

5.1.2. *Photoionization of hydrogen*

The reflection principle derived in section 5.1.1 does, of course, not only apply to molecules. An interesting example is its manifestation in the photoionization of the hydrogen atom, as was elaborated by Rost [65]. Consider this atom in its 1s state (ψ_{100}) interacting with an external electric field of unit field strength directed along the z axis, so that the atom–field interaction term is of the form $\mu = r\cos(\theta)$, where r, θ are polar coordinates. The total photoionization cross-section [66] then can be written in a time-dependent form as (employing atomic units in this section)

$$\sigma(\omega) \sim \int \exp(i\omega t) \langle r\cos(\theta)\psi_{100} | \exp(-i\hat{H}t) r\cos(\theta) \exp(i\hat{H}t) \psi_{100} \rangle \, dt. \tag{52}$$

Using the identity $\cos(\theta)\, Y_{00}(\theta, \varphi) = 1/3^{1/2} Y_{10}(\theta, \varphi)$, the angular part of the integral can be evaluated to yield the correlation function

$$c(t) = \tfrac{4}{3} \int r^3 \exp(-r) \exp(-i\hat{H}_1 t) r \exp(i\hat{H}_0 t) \exp(-r) \, dr, \tag{53}$$

where $\hat{H}_1$ and $\hat{H}_0$ differ in the centrifugal term $D(r) = r^{-2}$ which here takes the role of the difference potential. Neglecting the commutators between the kinetic energy operators and the coordinate-dependent functions yields

$$c(t) = \tfrac{4}{3} \int r^4 \exp(-2r) \exp[-iD(r)t] \, dr. \tag{54}$$

In evaluating the time integral appearing in the expression for the photoionization cross-section, a δ function is obtained which selects the particular r value where $D(r) = \omega$, that is $r = 1/\omega^{1/2}$. Thus we arrive at the expression

$$\sigma(\omega) \sim \frac{\exp(-2/\omega^{1/2})}{\omega^{-7/2}}. \tag{55}$$

Here the connection between the analytical expression for the cross-section and the hydrogen ground-state radial wavefunction is not so obvious. In particular the linearization of the difference potential, as used in the molecular case of section 5.1.1, is not possible. However, if the factor $1/\omega^{-3/2}$ which stems from the derivative of the

difference potential (see equation (49)) is accounted for, the remaining function $\rho(\omega)$ is of the form

$$\rho(\omega) = \frac{1}{\omega^2}\exp\left(-\frac{2}{\omega^{1/2}}\right), \tag{56}$$

which, using the relation between the radial coordinate r and ω, is identical with the radial probability density of the 1s state of hydrogen. Note, however, that there is an additional ω-dependent factor in the expression for the cross-section [66] which we did not include in the discussion.

5.2. *Transient spectroscopy*

We now shall discuss how the ideas outlined above relate to femtosecond time-resolved spectroscopy. There are several techniques which allow for a 'wave-packet mapping'. Let us shortly describe some of these.

(i) *Time-gated emission spectroscopy*. Here a pump–pulse prepares a non-stationary state in an excited electronic state of a molecule. After some time T, the frequency-resolved emission spectrum is detected. In doing so, one employs a short time window $b(t-T)$ centred around T. The idea is that the wave packet does not move essentially during the time interval defined by the window. As a result, the initial state in the emission process resembles a stationary state and the spectrum reflects the probability-density distribution in just the same way as an absorption spectrum does (see section 5.1.1). The calculation of the time- and frequency-resolved emission spectrum is straightforward but cumbersome [67–69]. The technique was applied in an experiment on the sodium dimer [70].

(ii) *Time-resolved kinetic energy time-of-flight* (*KETOF*) *spectroscopy*. In this case the wave-packet motion in a neutral electronic state is probed by excitation to a dissociative state of the molecular ion. Then the kinetic energy distribution of the ionic fragments is measured. Since the difference potential between the neutral and ionic electronic state depends, in general, on the bond distances (i.e. the ionization potential is coordinate dependent), ionization at different times, when the wave packet is located at different positions, yields different momentum distributions. The latter then reflect the coordinate dependence of the probability density. This was demonstrated by Assion *et al.* [71] using the Na_2 molecule. We note, that the theory to describe such experiments is very similar to what will be described below in connection with time-resolved photoelectron spectroscopy.

(iii) *Coulomb explosion spectroscopy*. Consider a wave packet which is the initial state for an ionization process in a diatomic molecule at a fixed time. If the laser pulse is short, the wave packet does not move during the ionization process. Employing an ultra-intense pulse results in multiple ionization (Coulomb explosion) so that the nuclei interact with each other through the unshielded Coulomb repulsion. The technique, in fact, is similar to the KETOF technique, that is the measured momentum distribution of the ions reflects the probability density of the initial wave packet [35, 72, 73]. Here the ionic potential is of the simple form $V_+(r) \sim 1/r$.

In what follows we shall, in detail, describe two methods to characterize nuclear wave packets.

5.2.1. *Time-resolved photoelectron spectroscopy*

The idea to employ time-resolved photoelectron spectroscopy to monitor molecular wave-packet dynamics was originally presented by Seel and Domcke [74, 75]. In their theoretical study they used a model for the vibrational motion in pyrazine on non-adiabatically coupled surfaces to illustrate that a photoelectron spectrum is an ideal observable to reveal details of the nuclear dynamics. Following this idea we investigated, in a series of papers [76–79], the simpler case of diatomic molecules. In the latter case, the idea of wave-packet mapping appears in a straightforward manner since only one internal coordinate, namely the atomic bond distance, is involved.

Let us return to our example as displayed in figure 1. The pump–pulse prepares a wave packet $|\psi_1(t)\rangle$ which moves outwards on a repulsive potential curve. The transition to the $|+\rangle$ state of the molecular ion (say, the ionic ground state) is induced by the time-delayed probe pulse. We now calculate the nuclear ionic wavefunction within the following approximations.

(i) The transition is treated within first-order perturbation theory.
(ii) The coupling between the electrons and the nuclei (Born–Oppenheimer approximation) and between the scattered photoelectron and the core electrons are neglected.

Under assumption (ii) the nuclear Hamiltonian of the ionic state is of the form

$$\hat{H}_+ = \hat{T} + V_+ + E, \tag{57}$$

where $\hat{T}$ is the kinetic energy operator of the nuclei, V_+ is the potential and E denotes the kinetic energy of the ejected photoelectron.

The nuclear ionic wavefunction is obtained as

$$|\psi_+(E,t)\rangle = \frac{i}{\hbar}\int_{-\infty}^{t} \exp\left[-i\left(\omega_2 - \frac{E}{\hbar}\right)t'\right] a_2(t') \exp\left(\frac{-i(\hat{T}+V_+)(t-t')}{\hbar}\right) \times \mu_{+1}(E) \exp\left(\frac{-i\hat{H}_1 t'}{\hbar}\right) |\psi_1(T)\rangle \, dt'. \tag{58}$$

Note that this expression is very similar to that obtained in the case of a neutral-to-neutral transition, that is equation (5). There are, however, two differences: firstly, the reduced frequency $\omega_2(E) = \omega_2 - E/\hbar$ enters into the integral and, secondly, the transition dipole moment now carries an additional dependence on the photoelectron energy. Whereas the latter dependence will be ignored in what follows (for a correct and much more involved treatment, see the recent papers by McKoy and co-workers [80, 81]), the first point is of great importance here, since for each reduced frequency a different nuclear ionic wavefunction is prepared.

The photoelectron spectrum, obtained at the delay time T, is defined as

$$P(E,T) = \lim_{t\to\infty} \langle \psi_+(E,t) | \psi_+(E,t) \rangle. \tag{59}$$

Here the time limit is obtained when the probe pulse stops interacting with the sample so that the ionic population remains constant. For completeness we note that the total ion yield is calculated as the integral of $P(E,T)$ over the electron energy.

A reflection principle is now derived using the arguments presented in the last section. Regarding times t after the probe pulse interaction and neglecting the commutators of $\hat{T}$ with the operators V_+ and μ_{+1}, the ionic wavefunction can be approximated as

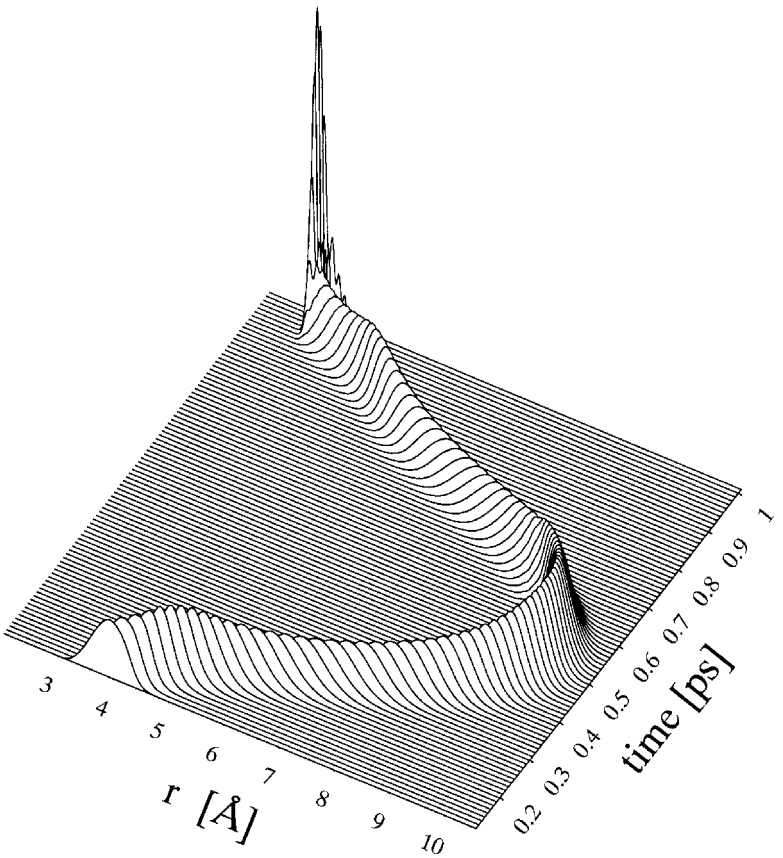

Figure 4. Vibrational wave-packet dynamics of Na_2 in its (2) $^1\Sigma_u^+$ state after femtosecond excitation. The modulus squared of the coordinate-dependent wave packet for one vibrational period is shown.

$$\psi_+(r,E,t) \sim \exp\left(\frac{-\mathrm{i}\hat{H}_+ t}{\hbar}\right)\int_{-\infty}^{\infty} \exp\left[-\mathrm{i}\left(\omega_2 - \frac{E}{\hbar} - \frac{D}{\hbar}\right)t'\right] a_2(t')\mu_{+1}\psi_1(r,T)\,\mathrm{d}t'. \quad (60)$$

Here, as before, $D = V_+ - V_1$ denotes the difference potential between the electronic states coupled in the probe transition. Evaluation of the time integral within the points r_i of stationary phase, that is where

$$D(r_i) - (\hbar\omega_2 - E) = 0, \quad (61)$$

yields the photoelectron spectrum as

$$P(E,T) \sim \sum_i |\mu_{+1}\psi_1(r_i,T)|^2. \quad (62)$$

We note that the stationary-phase approximation applied above is only of limited validity. In fact, since the time integral contains the pulse envelope (and thus is not proportional to a representation of the δ function) the photoelectron spectrum maps the probability density only within a 'low resolution'.

In the case when the difference potential is linear we find that, for a fixed probe frequency ω_2, the photoelectron spectrum regarded as a function of energy E directly reflects the probability density. In more detail, in the latter case only a single solution r_1 of equation (61) exists so that, in analogy to equation (51), we find that

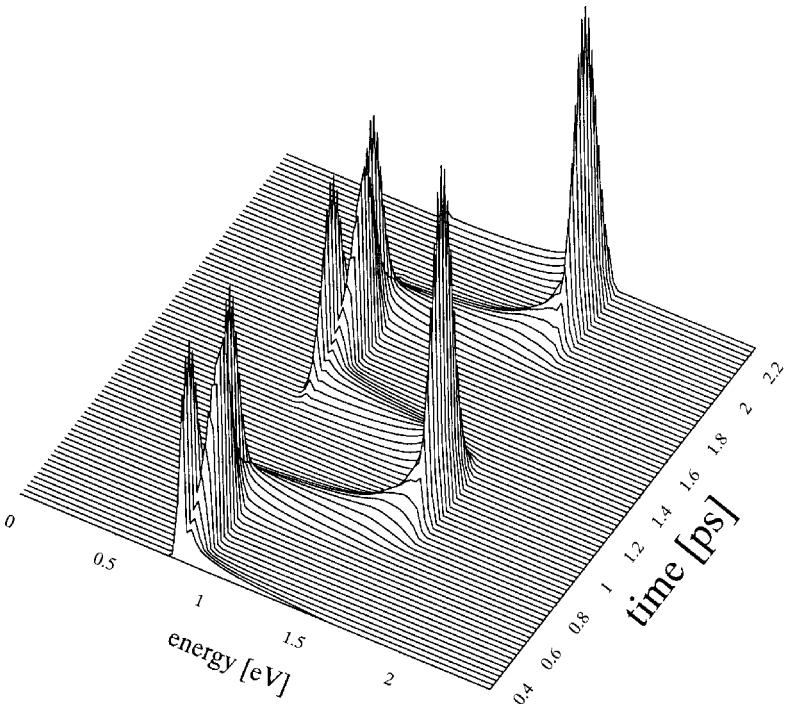

Figure 5. Time-resolved photoelectron spectra for photoionization of Na_2 out of the (2) $^1\Sigma_u^+$ state. The temporal changes of the spectrum reflect the vibrational motion as displayed in figure 4.

$$P(E, T) = |\mu_{+1}\,\psi_1(r_1, T)|^2. \tag{63}$$

Since now the wave packet $\psi_1(r, T)$ is a non-stationary state, different spectra are to be expected at different times, that is recording the electron kinetic energy distributions at different pump–probe delays enables us to monitor temporal changes of the probability density distribution.

Recently, several experiments have been performed employing time-resolved photoelectron spectroscopy to investigate the nuclear dynamics in molecules [82–90]. We would like to draw readers' attention to a beautiful experiment on the sodium dimer [91], which was the first direct conformation of the reflection principle in time-resolved photoelectron spectroscopy, as predicted theoretically earlier [76].

In our first numerical example to illustrate time-resolved photoelectron spectroscopy, we regard the femtosecond excitation of the sodium dimer to its (2) $^1\Sigma_u^+$ double-minimum state which has been studied by pump–probe ionization spectroscopy [71, 92]. The pump excitation to vibrational states above the potential barrier results in the preparation of a localized wave packet. The modulus squared of this packet is displayed in figure 4 covering an entire vibrational period. We note that it is also possible to prepare a superposition of states with energies below the potential barrier, resulting in quite different wave-packet dynamics [77].

Calculated photoelectron spectra are shown in figure 5 as a function of pump–probe delay. The temporal changes in the energy distribution nicely reflect the wave packet's vibrational motion. In particular, the difference potential here is such that an inward motion of the wave packet results in the shift of the spectrum towards higher photoelectron kinetic energies. An additional structure which is not apparent in

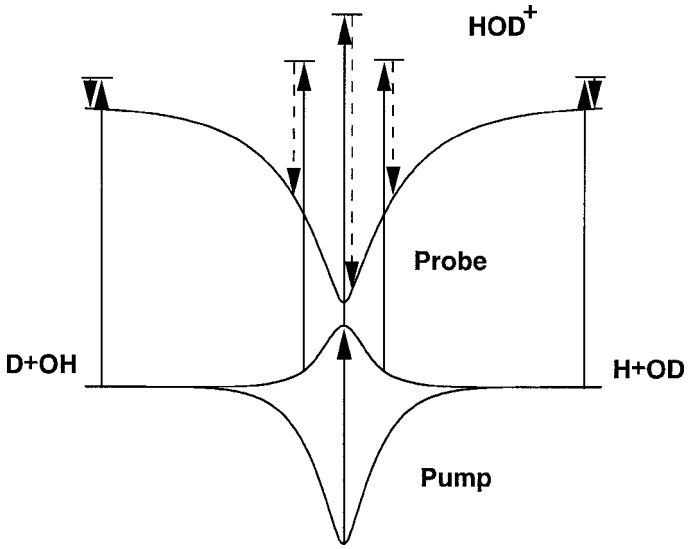

Figure 6. H_2O pump–probe ionization scheme showing cuts of potential surfaces corresponding to the electronic ground state, an excited state and the ionic ground state as a function of the reaction coordinate in the intermediate state. The solid arrows indicate the pump and probe wavelengths. The lengths of the broken arrows indicate the energies, where maxima in the photoelectron spectra are expected if ionization occurs at different times during the fragmentation process.

figure 4 arises because the difference potential is not monotonic at smaller bond lengths.

In passing, we note that our calculation assumed a constant transition dipole moment μ_{+1}. Since the potential barrier is caused by non-adiabatic coupling between different electronic states, this approximation breaks down. However, the overall picture presented here is correct, as can be seen by comparison with recent work [80, 81].

Let us now turn to a second example. Figure 6 illustrates a pump–probe ionization experiment for the HOD molecule [93]. Cuts through the potentials of different electronic states are drawn along the reaction coordinate s of the dissociative intermediate state. Here the pump excitation is from the electronic ground (X) to the first electronically excited state (A). This state is purely repulsive leading to H+OD and D+OH fragments. The probe process results in the preparation of HOD^+ in its electronic ground state. Let us, in what follows, use the same notation as before, namely $|0\rangle$, $|1\rangle$ and $|+\rangle$ for the three electronic states. The solid arrows in the figure indicate the centre frequencies of pump and probe pulses. The broken arrows, on the other hand, indicate photoelectron energies E which fulfil the resonance condition $V_+(s) - V_1(s) - (\omega_2 - E) = 0$.

The dynamics of the fragmentation are illustrated in figure 7 which displays contour lines of the potential $V_1(R_H, R_D)$ as a function of the OH (OD) distance $R_H(R_D)$. The bending angle of the molecule has been fixed to a value of 104° corresponding to the equilibrium angle in the electronic ground state. It has been shown that the fragmentation process starting from the rovibrational ground state in $|0\rangle$ is nearly independent of the bonding angle [64]. This allows for a realistic simulation using a fixed value for this coordinate.

The dynamics of a wave packet created with a pulse of 12 fs width and a centre

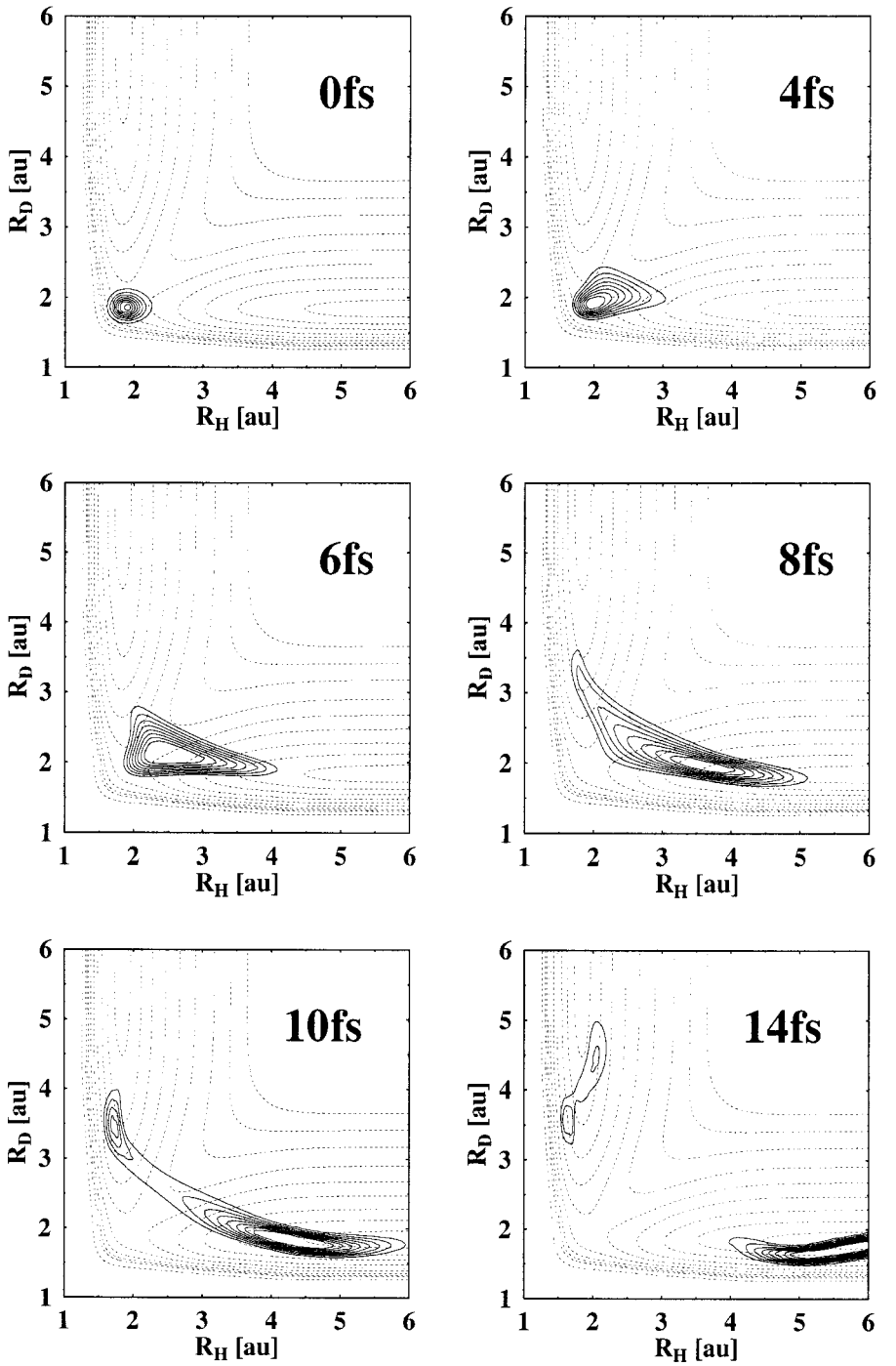

Figure 7. H_2O fragmentation dynamics upon femtosecond excitation. Contours of the potential surface of the dissociative electronic state are displayed as a function of the OH (R_H) and OD (R_D) distances. Also shown is the modulus squared of the wave packet prepared in the pump process at different times, as indicated. The dissociation into the two reaction channels (D+OH, H+OD) is seen in the bifurcation of the wave packet.

frequency corresponding to 8 eV (maximum of the absorption band) is also illustrated in figure 7, which shows contours of the probability density at different times. Here the value of 0 fs corresponds to the centre of the pump pulse. At early times, the wave packet $\psi_1(R_H, R_D)$ is prepared on top of the reaction barrier of the potential V_1. In the course of the fast dissociation process a bifurcation occurs, resulting in two packets moving into the different reaction channels.

It is clear that the reflection principle here cannot yield a complete picture of the probability density. The resonance condition which establishes the connection between $|\psi_1|^2$ and the photoelectron spectrum in our two-dimensional model is

$$D(R_H, R_D) - (\omega_2 - E) = 0. \tag{64}$$

Thus, in contrast with the diatomic case, there are several points (R_H^i, R_D^i) for which equation (64) holds (in fact, equation (64) defines complete one-dimensional cuts through the two-dimensional difference potential). Nevertheless, the two wave packets move essentially along the reaction coordinate and it is to be expected that the time-resolved photoelectron spectrum maps the wave-packet motion along the reaction path. This is indeed the case in our example, as can be observed from figure 6. The displayed spectra were calculated using a probe pulse of the same width as the pump pulse and a frequency corresponding to an energy of 12 eV. The figure contains results for H_2O and its isotopes. In each case, one can nicely see traces of the wave-packet dynamics. Since the difference potential increases with increasing values of the reaction coordinate s (figure 8), the spectra shift from higher to smaller energies. For times up to 10 fs the spectra reflect the spreading of the packet. For long delay times the spectrum will converge to a curve representing the spectral width of the probe pulse. The reason for this behaviour is that in the asymptotic region the difference potential along the reaction path becomes constant so that the time integral (60) is independent of s and, when it is considered as a function of the photoelectron energy E, is the Fourier transform of the pulse-envelope function, that is the pulse envelope in the energy domain. Note, however, that in general the photoelectron spectrum will reflect the vibrational motion of the fragments. The photofragmentation of water is a very fast process and to obtain the spectra, as shown above, one needs very short pulses with large frequencies. A measurement of the pump–probe photoelectron distributions has not been performed to date; we note, however, that recently a pump–probe ionization experiment on the water molecule indeed has been carried through [94].

5.2.2. *Integrated pump–probe fluorescence spectroscopy*

Time-resolved photoelectron spectroscopy, as discussed in section 5.2.1, requires the recording of a two-dimensional signal as a function of the delay time T and the photoelectron energy E. In what follows we want to show that pump–probe fluorescence spectroscopy, as discussed in the first part of this review, is also able to yield information about radial probability densities although the corresponding signal is recorded as a function of only a single parameter, namely the delay time. In particular, we treat the pump–probe process illustrated in figure 1. In the case of fragment detection (see sections 2.2 and 3.3) the signal is approximately given by equation (33). In order to relate the pump–probe signal to the probability density distribution $\rho_1(r, T) = |\psi_1(r, T)|^2$ we evaluate the time derivative of the signal to obtain [95]

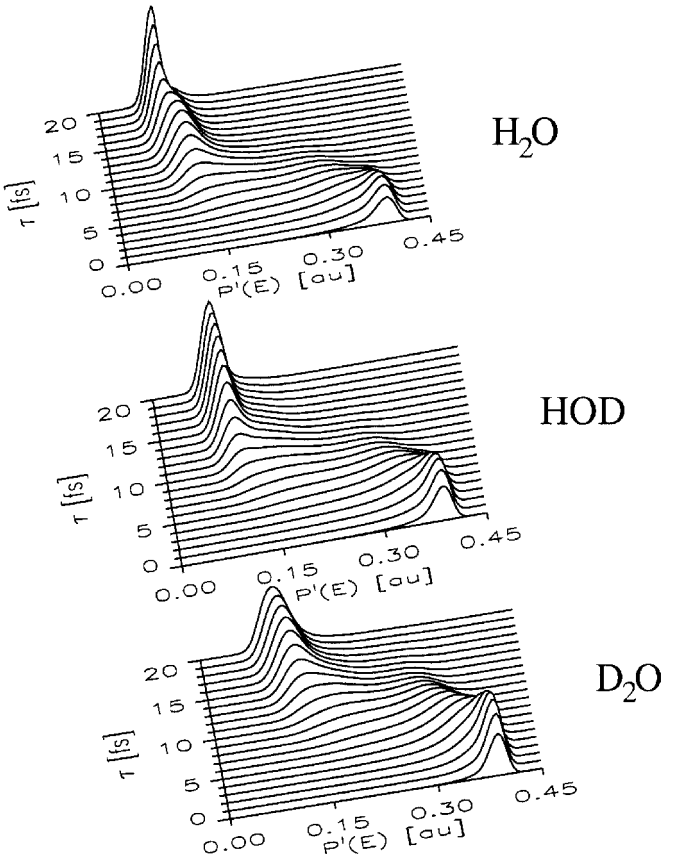

Figure 8. Time-resolved photoelectron spectra for water isotopes. The shift of the spectra towards lower energy as a function of time reflects the motion of the wave packets along the reaction coordinate into the reaction channels as illustrated in figure 7.

$$\frac{\mathrm{d}}{\mathrm{d}T}P(T) = \int_{r_\mathrm{p}}^{\infty} \psi_1^*(r,T)\frac{\mathrm{d}}{\mathrm{d}T}\psi_1(r,T)\,\mathrm{d}r + \mathrm{CC}, \tag{65}$$

where CC is the complex conjugate. Assuming that the pump pulse stopped interacting with the sample, the wave packet ψ_1 propagates unperturbed so that

$$\frac{\mathrm{d}}{\mathrm{d}T}P(T) = \int_{r_\mathrm{p}}^{\infty} \psi_1^*(r,T)\left(\frac{-\mathrm{i}}{\hbar}\right)\hat{H}_1\,\psi_1(r,T)\,\mathrm{d}r + \mathrm{CC}. \tag{66}$$

In the asymptotic region ($r > r_\mathrm{p}$) the Hamiltonian H_1 equals the kinetic-energy operator (except for a constant which does not change the following considerations and is dropped in what follows). Thus we arrive at the equation

$$\frac{\mathrm{d}}{\mathrm{d}T}P(T) = \frac{\mathrm{i}\hbar}{2m}\int_{r_\mathrm{p}}^{\infty} \psi_1^*(r,T)\frac{\mathrm{d}^2}{\mathrm{d}r^2}\psi_1(r,T)\,\mathrm{d}r + \mathrm{CC}. \tag{67}$$

The integral can be evaluated resulting in the expression

$$\frac{\mathrm{d}}{\mathrm{d}T}P(T) = \frac{\hbar}{2m\mathrm{i}}\left(\psi_1^*(r,T)\frac{\mathrm{d}}{\mathrm{d}r}\psi_1(r,T) - \psi_1(r,T)\frac{\mathrm{d}}{\mathrm{d}r}\psi_1^*(r,T)\right)_{r_\mathrm{p}}, \tag{68}$$

where the subscript indicates that the expression has to be evaluated at $r = r_p$. Thus, the time derivative of the signal equals the probability flux $j(r_p, T)$ through the point $r = r_p$. Although $(d/dt)\ P(T)$ does not directly reflect the probability density at a certain point in time, it is very much related to it. Rewriting the wavefunction in terms of the density ρ_1 [96], that is

$$\psi_1(r, T) = [\rho_1(r, T)]^{1/2} \exp\left(\frac{iS(r, T)}{\hbar}\right), \tag{69}$$

with a real function $S(r, T)$, the signal takes the form

$$\frac{d}{dT}P(T) = \frac{\hbar}{m}\left(\rho_1(r, T)\frac{d}{dr}S(r, T)\right)_{r_p}. \tag{70}$$

If the function $S(r, T)$ depends only weakly on time, the signal indeed is proportional to the probability density passing through r_p. Analytical considerations show that the time dependence of $S(r, T)$ is weak for large mass and available energy [95]. The above connection enables us to determine ρ_1 as a function of distance, as will be demonstrated below using a numerical example.

Let us, at this point, comment on the general multidimensional (N-dimensional) case. Here the mapping is, of course, not unique in the sense that a signal recorded as a function of one parameter cannot reflect a density depending on many coordinates. This was already discussed regarding the photoelectron spectroscopy of the water molecule in section 5.2.1. Using the concept of a reaction coordinate (as for the photodissociation of water) the $N-1$ remaining degrees of freedom can be integrated out and the flux-mapping procedure will give, to a good approximation, a cut of the moving wave packet along this coordinate.

Let us, for completeness, discuss the fluorescence signals arising from the detection of the wave packet in the inner potential region (transition-state detection, section 2.1). To a good approximation we can represent the Franck–Condon window function by a square window of width $2d$:

$$F[D(r) - \omega_2] = \mu_{21}\,\theta[r - (r_p - d)]\,\theta[(r_p + d) - r]. \tag{71}$$

Evaluating, as above, the time derivative of the signal we obtain the expression

$$\frac{d}{dT}P(T) = j(r_p - d, T) - j(r_p + d, T). \tag{72}$$

Here we assumed that the potential $V_1(r)$ is constant over the interval $[r_p - d, r_p + d]$. Thus, we measure the difference in fluxes at two spatial points for a given time. In the limit that these points are sufficiently close, we may write

$$\begin{aligned}\frac{d}{dT}P(T) &\sim (2d)\frac{j(r_p - d, T) - j(r_p + d, T)}{2d} \\ &\sim -2d\left(\frac{d}{dr}j(r, T)\right)_{r_p} \\ &= 2d\frac{d}{dT}\rho_1(r_p, T),\end{aligned} \tag{73}$$

where the last equality follows from the continuity equation satisfied by $\rho_1(r, t)$ [96]. Integrating over time, one finds the equation

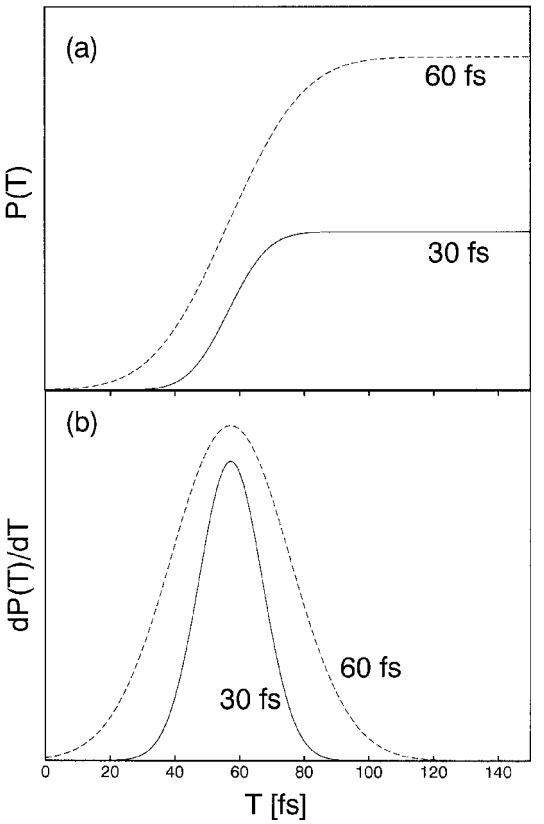

Figure 9. (*a*) Calculated pump–probe signals in the case of fragment detection and (*b*) the respective time derivatives. Signals are shown for pump pulses of 30 and 60 fs width, as indicated. In each case, the time derivatives resemble the probability density at the inner boundary r_p of the Franck–Condon window at delay time T.

$$P(T) \sim 2d\rho_1(a, T), \tag{74}$$

which alternatively can be inferred from equation (13) within the same approximations. Thus, in the case of a transition-state detection and for a narrow Franck–Condon window, the density can be directly correlated to the pump–probe signal.

Figure 9(*a*) displays pump–probe signals calculated for two different widths of a Gaussian pump pulse. In calculating the signal we employed equation (33). The frequency was set to 4.6 eV which corresponds to excitation in the vicinity of the absorption maximum. In both cases the time $T = 0$ corresponds to the maximum of the respective pump pulse. The typical increase from zero to a constant is seen, reflecting the motion of the wave packet into the excitation window (see section 3.3).

The time derivatives of the signals (figure 9(*b*)) are both Gaussian-like curves. We shall now map these curves into coordinate space using the procedure described above. Since the wave packets are located in the asymptotic region, they move with a constant speed towards larger distances. We assume the expectation value of the energy to be $\langle\psi_1|H_1|\psi_1\rangle = \omega_1 - V_1(r = \infty)$, which reflects energy conservation in the limit of long pulses. The velocity v_0 is given by $v_0 = [2[\omega_1 - V_1(r = \infty)]/m]^{1/2}$ Using this value, the r-dependent density can be obtained as

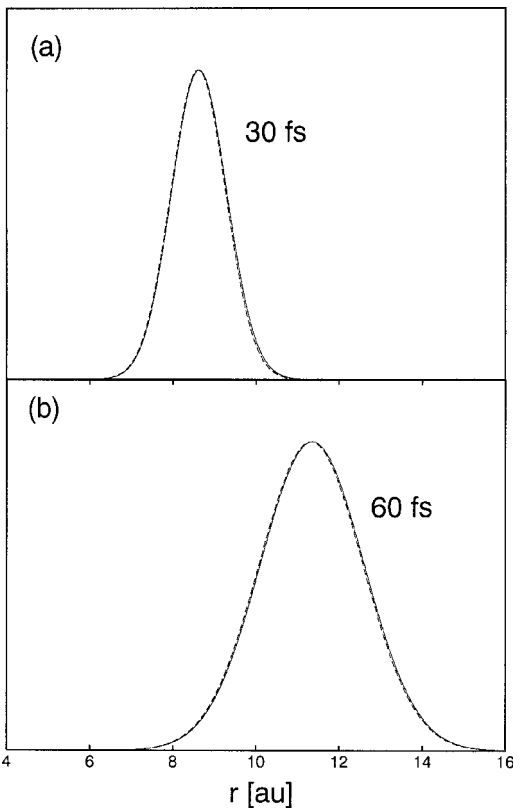

Figure 10. Constructed (——) and numerically calculated (– – –) wavefunctions (absolute square): (*a*) 30 fs excitation; (*b*) 60 fs excitation (see figure 9).

$$\rho_1(r_p + v_0 t, T) \sim \left(\frac{d}{d\lambda} P(\lambda)\right)_{\lambda = T - t}. \tag{75}$$

In performing the construction of the wave-packet density it should be clear that, in order to obtain it in its entirety, the wave packet must have passed completely the point r_p.

Figure 10 compares the exact calculated densities $\rho_1(r, t)$ with the densities inverted from the signals. Here we used pulses of 30 fs (60 fs) width and equation (75) was applied 140 fs (180 fs) after the maximum of the respective pump pulse. The different curves for the two pulse lengths are hardly distinguishable. This confirms that indeed the probability-density amplitudes can be inverted from the pump–probe fluorescence signal and the time dependence of the phase function $(d/dr) S(r, T)$ is negligible in our example.

One has to keep in mind that the outgoing wave packet spreads in coordinate space. The spreading cannot be determined from the signal. However, this would in principle be possible if excitation to another excited electronic state at a different critical distance r_p could be achieved. Furthermore the distance r_p is, in general, not precisely known. In this case the r-dependent density can be determined from an experimental signal within an unknown shift on the r axis only.

5.2.3. *Phase retrieval*

Above we have described two methods to obtain the coordinate-dependent

probability density prepared by a femtosecond pulse. Quantum mechanics uses complex-valued wavefunctions to predict the outcome of measurements. We now pose the question of whether it is possible to determine the phase of the wavefunction. This 'phase-retrieval' problem has been discussed extensively; see for example [97–100] for theoretical work and [101, 102] for experimental work. Our starting point will be the density distribution in coordinate and momentum space. Already Pauli [103] was concerned with the question of whether knowledge of these densities is sufficient to determine the complex-valued wavefunction. The same question arises in microscopy where intensity distributions in image and diffraction planes are measured [104–107]. Below we present an iterative scheme originally proposed by Gerchberg and Saxton [104] which allows for the characterization of the wavefunction from the density distributions in coordinate and momentum space. Thus, it is necessary to outline methods to obtain the momentum-space density. This will be done for the specific example of the photofragmentation of a diatomic molecule, as is illustrated in figure 1.

In the case that we refer to, the pump excitation results in photofragments with different momenta. In what follows we shall drop the subscript 1, indicating the wavefunctions, the propagator, etc., belonging to the electronic state $|1\rangle$. The fragment momentum distribution $\rho(p)$ is the projection of the wave packet on momentum eigenstates $|\psi_p\rangle$ with relative kinetic energies $E_p = p^2/2m$:

$$\rho(p) = \lim_{t\to\infty} |\langle \psi_p | \psi(t)\rangle|^2 = \lim_{t\to\infty} |\psi(p,t)|^2. \tag{76}$$

Thus $\rho(p)$ equals the absolute square of the momentum-space wavefunction. This distribution can be determined by a KETOF measurement, see the beginning of section 5.2. We shall not discuss the question of the experimental resolution which is important to estimate the accuracy of the phase construction; rather the following discussion is focused on the basic principles; for more details see [108].

The momentum-space density is measured in the limit of long times, but $\rho(p,t)$ remains unchanged while the wave packet moves through the region where the potential $V(r)$ is constant. Hence we can think of the measured $\rho(p)$ and $\rho(r)$ as belonging to the same time t_0, the time when $\psi(r) \equiv \psi(r,t_0)$ and $\psi(p) \equiv \psi(p,t_0)$ have just entered the asymptotic region. It is worthwhile to mention that the measurement of the KETOF spectrum is not the only possible experimental method to obtain the momentum-space density. Projection of the first-order state (2) on to the scattering states $|\psi_p -\rangle$ of energy E_p yields, for times t after the pump excitation is finished [109], the expression

$$\langle \psi_p - |\psi(t)\rangle = \exp\left(\frac{-\mathrm{i}E_p t}{\hbar}\right) \langle \psi_p - |\mu_{10}|\psi_0\rangle\, I(E_p), \tag{77}$$

with the integral

$$I(E_p) = \int_{-\infty}^{+\infty} a(t') \exp\left(\frac{\mathrm{i}E_p t'}{\hbar}\right) \mathrm{d}t'. \tag{78}$$

We now concentrate on a time t_0 where the state $|\psi(t)\rangle$ is completely localized in the asymptotic region. Inserting the definition of $|\psi_p -\rangle$ in terms of the Møller operator Ω_- [110], one finds that

$$\langle \psi_p - |\psi(t_0)\rangle = \langle \Omega_- \psi_p | \psi(t_0)\rangle = \langle \psi_p | \Omega_-^\dagger \psi(t_0)\rangle, \tag{79}$$

where

$$\Omega_-^\dagger = \lim_{t\to+\infty} [U_0^\dagger(t)\, U(t)], \tag{80}$$

and $U_0(t)$ is the free-particle propagator. Since $|\psi(t_0)\rangle$ is localized in the interaction-free region $\Omega_-^\dagger$ is the unit operator. Noting furthermore that $|\langle\psi_p - |\mu|\psi_0\rangle|^2$ is proportional to the absorption cross-section [64] $\sigma(\omega)$ (where $\omega = \varepsilon_0 + E_p$; see section 5.1.1) we finally find the asymptotic momentum distribution

$$|\langle\psi_p|\psi(t_0)\rangle|^2 = |\psi(p, t_0)|^2 \sim \sigma(E_p)\, |I(E_p)|^2. \tag{81}$$

The last equation relates the momentum-space density to the product of the absorption cross-section and the spectral distribution of the pump pulse. Thus a measurement of $\sigma(E_p)$ can provide the momentum distribution if the employed laser pulse is well characterized.

The experiments described above allow, at least in principle, for a determination of the densities $\rho(p) = |\psi(p)|^2$ (see this section) and $\rho(r) = |\psi(r)|^2$ (see section 5.2.2). It is immediately clear that two wavefunctions $\psi(r)$ and $\exp(i\phi)\,\psi(r)$ have the same densities if ϕ is a constant, that is sole knowledge of the densities does not fix the overall phase, which is, however, irrelevant in quantum mechanics. Besides that, wavefunctions with a non-trivial phase difference can also yield identical densities [105, 106]. The mathematical conditions to find a unique (up to an overall phase factor) solution have been worked out [106]. Without going into mathematical details, we note that, in our case of photofragmentation, the scheme which will be presented below indeed converges to the correct wavefunction; for details see [108].

We shall now describe an iterative scheme to find the complex-valued wavefunction from the known densities. Note that a similar scheme has been employed in the inversion of potential curves from experimental data [111].

Denoting the experimentally determined functions as $a(p)$ and $a(r)$, the scheme is started as (equivalently the momentum-space density could serve as starting point)

$$\psi_0(r) = a(r), \tag{82}$$

and the Fourier transform of this function yields $\tilde{\psi}_0(p)$. Next we calculate

$$\tilde{\psi}_1(p) = a(p)\frac{\tilde{\psi}_0(p)}{|\tilde{\psi}_0(p)|}. \tag{83}$$

Taking the Fourier transform yields $\psi_1(r)$, which is used to calculate

$$\psi_2(r) = a(r)\frac{\psi_1(r)}{|\psi_1(r)|}. \tag{84}$$

This iteration scheme may be continued until convergence is achieved. A measure for the deviation of the iterated coordinate-space amplitude from the exact amplitude is given by

$$\delta_n = \int [|\psi(r)| - |\psi_n(r)|]^2\, \mathrm{d}r. \tag{85}$$

Gerchberg and Saxton [104] have shown that the iteration is stable in the sense that δ_n cannot increase with increasing n (considering only odd n because, for even n, δ_n equals zero by construction).

In a numerical application we employ the same model for the dissociation of the

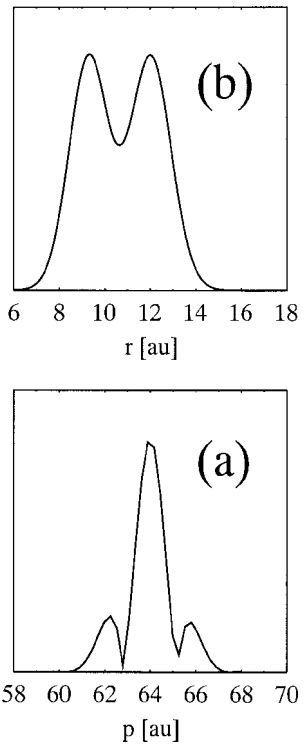

Figure 11. (*a*) Coordinate-space and (*b*) momentum-space densities for the excitation with two time-delayed Gaussian pump pulses. The densities were calculated at a time when the wave packet entered the asymptotic region.

ICN molecule, as was discussed earlier in this review. We calculated wavefunctions for a pump excitation with a pulse envelope consisting of the sum of two Gaussians of 30 fs width, which are delayed with respect to each other by $T = 40$ fs. This results in the coordinate-space wave packet as displayed in figure 11 (*a*). Here the momentum-space density exhibits a characteristic structure (figure 11 (*b*)) which can be understood as follows: two wave packets $|\varphi(t)\rangle$ and $|\varphi(t-T)\rangle$ are created by identical but delayed pulses; the asymptotic fragment distribution then is

$$\rho(p) = \lim_{t\to\infty} |\langle \psi_p | [|\varphi(t)\rangle + |\varphi(t-T)\rangle]|^2. \tag{86}$$

This expression can be evaluated in a momentum space as

$$\rho(p) = |\varphi(p)|^2[2+2\cos(E_p T)]. \tag{87}$$

Thus $\rho(p)$ contains an interference term causing the structure seen in figure 11 (*b*). This is analogous to a two-slit experiment; in our case the separation of the slits corresponds to the pulse-delay T [112].

Using the densities displayed in figures 11 (*a*) and (*b*) as input in the Gerchberg–Saxton algorithm we arrived at the functions displayed in figure 12. The figure contains the real parts of the spatial wavefunctions obtained after n iterations. In the figure for $n = 9$ the real part of the numerically exact wavefunction (the target wavefunction) is also plotted. It is nearly identical with the iterated function. Of course, the functions will, in general, differ by an overall phase factor which we

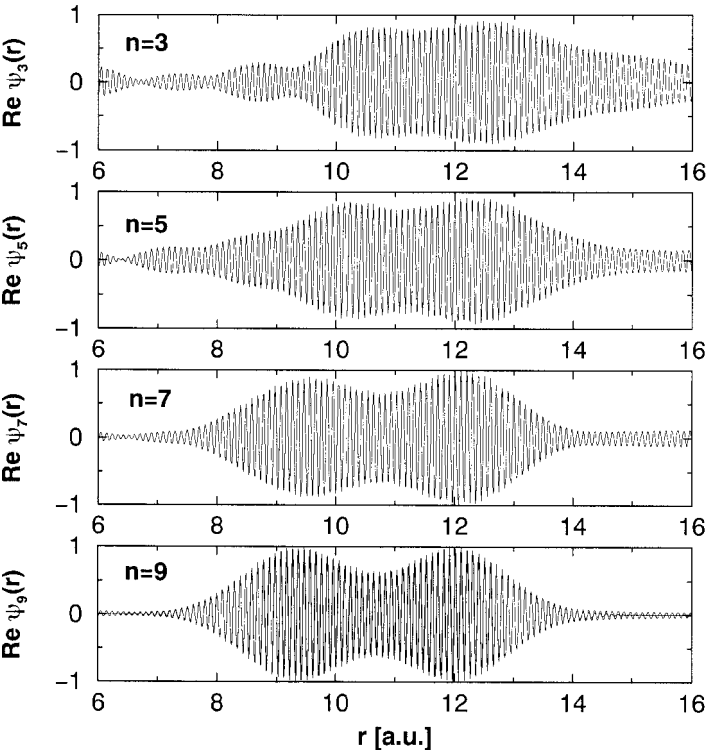

Figure 12. Real part of the coordinate-space wavefunction constructed from the coordinate and momentum densities after n iteration steps, as indicated. The figure for $n = 9$ contains the numerically exact function.

eliminated by fixing the phase of both functions to be the same at a particular value of r. We note that the imaginary part of the wavefunctions shows a similar convergence behaviour.

6. Summary

We have reviewed the relation between femtosecond time-resolved pump–probe signals and nuclear wave-packet motion in molecules. In doing so, three levels of 'state probing' were highlighted, namely the detection of temporal changes in, firstly, the average position, secondly, the probability density and, thirdly, the wave packet itself including its complex-valued phase.

The focus was on the detection via the total frequency integrated pump–probe fluorescence signal and via time-resolved photoelectron spectroscopy.

For detection via the pump–probe fluorescence signal, we discussed the connection between the time delay and the average position of the wave packet created by the pump pulse. Furthermore, we elaborated on how to deconvolute the 'blurring' of the signal due to pump pulses with a finite temporal width.

We showed how time-resolved photoelectron spectroscopy can be used in order to obtain the temporal change in the nuclear probability density. Here the kinetic energy distribution of the photoelectrons, detected at a certain delay time is a direct measure of the coordinate-dependent density at that particular time.

Whereas photoelectron spectroscopy needs the recording of a spectrum as a function of two parameters (namely energy and delay time), integrated pump–probe fluorescence signals are detected as a function of delay time only. We have

demonstrated that this method is also capable of characterizing nuclear probability densities. In the case of fragment detection in a unimolecular reaction, the time derivative of the signal is a measure of the nuclear density (as a function of the reaction coordinate), entering the asymptotic reaction channel.

As a final application of femtosecond time-resolved spectroscopy we demonstrated that, by combination of various techniques, it is possible to characterize nuclear wave packets including their complex phase.

Acknowledgements

Financial support by the Deutsche Forschungsgemeinschaft and the Fonds der Chemischen Industrie is gratefully acknowledged. V.E. expresses his thanks to M. Braun, M. Erdmann, C. Meier and M. Lein who contributed significantly to the work reported here.

References

[1] Zewail, A. H., 1994, *Femtochemistry*, Vols 1, 2 (Singapore: World Scientific).
[2] Manz, J., and Wöste, L. (editors), 1995, *Femtosecond Chemistry* (Weinheim: VCH).
[3] Chergui, M. (editor), 1996, *Femtochemistry* (Singapore: World Scientific).
[4] Sundström, V. (editor), 1997, *Femtochemistry and Femtobiology* (London: Imperial College Press).
[5] Gaspard, P., and Burghardt, I. (editors), 1997, *Adv. chem. Phys.*, **101**.
[6] Zewail, A. H., 2000, *J. phys. Chem.*, **104**, 5660.
[7] Bersohn, R., and Zewail, A. H., 1988, *Ber. Bunsenges. phys. Chem.*, **92**, 373.
[8] Williams, S. O., and Imre, D. G., 1988, *J. phys. Chem.*, **92**, 6648.
[9] Lee, S.-Y., Pollard, W. T., and Mathies, R. A., 1989, *Chem. Phys. Lett.*, **163**, 11.
[10] Yan, Y. J., Fried, L. E., and Mukamel, S., 1989, *J. phys. Chem.*, **93**, 8149.
[11] Fried, L. E., and Mukamel, S., 1990, *J. chem. Phys.*, **93**, 3063.
[12] Engel, V., Metiu, H., Almeida, R., Marcus, R. A., and Zewail, A. H., 1988, *Chem. Phys. Lett.*, **152**, 1.
[13] Engel, V., and Metiu, H., 1989, *J. chem. Phys.*, **90**, 6116.
[14] Heather, R., and Metiu, H., 1989, *Chem. Phys. Lett.*, **157**, 505.
[15] Choi, S. E., and Light, J. C., 1989, *J. chem. Phys.*, **90**, 2593.
[16] Fain, B., Lin, S. H., and Hamer, N., 1989, *J. chem. Phys.*, **91**, 4485.
[17] Lee, S.-Y., Pollard, W. T., and Mathies, R. A., 1989, *J. chem. Phys.*, **90**, 6146.
[18] Krause, J. L., Shapiro, M., and Bersohn, R., 1991, *J. chem. Phys.*, **94**, 5499.
[19] Lee, S.-Y., 1995, *Femtosecond Chemistry*, edited by J. Manz and L. Wöste (Weinheim: VCH), chapter 2.
[20] Braun, M., Meier, C., and Engel, V., 1995, *J. chem. Phys.*, **103**, 7907.
[21] Li, Z., Fang, J.-Y., and Martens, C. C., 1996, *J. chem. Phys.*, **104**, 6919.
[22] de Vivie-Riedle, R., Kobe, K., Manz, J., Meyer, W., Reischl, B., Rutz, S., Schreiber, E., and Wöste, L., 1996, *J. phys. Chem.*, **100**, 7789.
[23] Reischl, B., de Vivie-Riedle, R., Rutz, S., and Schreiber, E., 1996, *J. chem. Phys.*, **104**, 8857.
[24] Hiller, E. M., and Cina, J. A., 1996, *J. chem. Phys.*, **105**. 3419.
[25] Cao, J., and Wilson, K. R., 1997, *J. chem. Phys.*, **106**, 5062.
[26] Dietz, H., and Engel, V., 1998, *J. phys. Chem.*, A, **102**, 7406.
[27] Shen, Y., and Cina, J. A., 1999, *J. chem. Phys.*, **110**, 9793.
[28] Dilthey, S., Hahn, S., and Stock, G., 2000, *J. chem. Phys.*, **112**, 4910.
[29] Mukamel, S., 1995, *Principles of Nonlinear Optical Spectroscopy* (Oxford University Press).
[30] Pollard, W. T., and Mathies, R. A., 1992, *A. Rev. phys. Chem.*, **43**, 497.
[31] Zinth, W., and Kaiser, W., 1993, *Ultrashort Laser Pulses*, second edition, edited by W. Kaiser (New York: Springer), Chapter 6.
[32] Baumert, T., and Gerber, G., 1995, *Adv. atom. molec. opt. Phys.*, **35**, 163.
[33] Domcke, W., and Stock, G., 1997, *Adv. chem. Phys.*, **100**, 1.
[34] Ungar, L. W., and Cina, J. A., 1997, *Adv. chem. Phys.*, **100**, 171.

[35] CORKUM, P. B., IVANOV, M. YU., and WRIGHT, J. S., 1997, *A. Rev. phys. Chem.*, **48**, 387.
[36] MATERNY, A., CHEN, T., SCHMITT, M., SIEBERT, T., VIERHEILIG, A., ENGEL, V., and KIEFER, W., 2000, *Appl. Phys.* B, **71**, 299.
[37] HENRIKSEN, N. E., 1995, *Adv. chem. Phys.*, **91**, 433.
[38] MEIER, C., and ENGEL, V., 1995, *Femtosecond Chemistry*, edited by J. Manz and L. Wöste (Weinheim: VCH), chapter 11.
[39] LAX, M., 1952, *J. chem. Phys.*, **20**, 1752.
[40] MØLLER, K. B., HENRIKSEN, N. E., and ZEWAIL, A. H., 2000, *J. chem. Phys.*, **113**, 10477.
[41] MEYER, S., MEIER, C., and ENGEL, V., 1998, *J. chem. Phys.*, **108**, 7631.
[42] DANTUS, M., ROSKER, M. J., and ZEWAIL, A. H., 1987, *J. chem. Phys.*, **87**, 2395.
[43] ROSKER, M. J., DANTUS, M., and ZEWAIL, A. H., 1988, *Science*, **241**, 1200.
[44] HENRIKSEN, N. E., and ENGEL, V., 1999, *J. chem. Phys.*, **111**, 10469.
[45] JANSZKY, J., and VINOGRADOV, A. V., 1990, *Phys. Rev. Lett.*, **64**, 2771.
[46] AVERBUKH, I., and SHAPIRO, M., 1993, *Phys. Rev.* A, **47**, 5086.
[47] HELLER, E. J., 1975, *J. chem. Phys.*, **62**, 1544.
[48] MØLLER, K. B., and HENRIKSEN, N. E., 1996, *J. chem. Phys.*, **105**, 5037.
[49] CHAMPENEY, D. C., 1973, *Fourier Transforms and their Physical Applications* (London: Academic Press).
[50] ROSKER, M. J., DANTUS, M., and ZEWAIL, A. H., 1988, *J. chem. Phys.*, **89**, 6113.
[51] HERZBERG, G., 1950, *Molecular Spectra and Molecular Structure I, Spectra of Diatomic Molecules* (New York: Van Nostrand).
[52] TELLINGHUISEN, J., 1985, *Photodissociation and Photoionization*, edited by K. P. Lawley (New York: Wiley).
[53] KOLBA, E., MANZ, J., SCHREIER, H. J., and TRISCA, I., 1992, *Chem. Phys. Lett.*, **189**, 505.
[54] VOGT, P., SCHMITT, M., and KIEFER, W., 1995, *Chem. Phys. Lett.*, **243**, 64.
[55] LEE, S.-Y., 1993, *Chem. Phys. Lett.*, **203**, 93.
[56] EICHELSDÖRFER, M., and ENGEL, V., 1996, *Chem. Phys. Lett.*, **263**, 640.
[57] EICHELSDÖRFER, M., and ENGEL, V., 1997, *J. Raman Spectrosc.*, **28**, 427.
[58] SCHINKE, R., 1986, *J. chem. Phys.*, **85**, 5049.
[59] HENNIG, S., ENGEL, V., and SCHINKE, R., 1986, *J. chem. Phys.*, **84**, 5444.
[60] MERZBACHER, E., 1998, *Quantum Mechanics*, third edition (New York: Wiley).
[61] GORDON, R. G., 1968, *Adv. magn. Reson.*, **3**, 1.
[62] HELLER, E. J., 1981, *Accts chem. Res.*, **14**, 368.
[63] HELLER, E. J., 1978, *J. chem. Phys.*, **68**, 2066.
[64] SCHINKE, R., 1993, *Photodissociation Dynamics* (Cambridge University Press).
[65] ROST, J. M., 1995, *J. Phys.* B, **28**, L601.
[66] STARACE, A. F., 1996, *Atomic, Molecular, and Optical Physics Handbook*, edited by G. W. F. Drake (Woodbury: AIP Press), chapter 24.
[67] EBERLY, J. H., and WODKIEWICZ, K., 1979, *J. opt. Soc. Am.*, **67**, 1252.
[68] KOWALCZYK, P., RADZEWICZ, C., MOSTOWSKI, J., and WALMSLEY, I. A., 1990, *Phys. Rev.* A, **42**, 5622.
[69] SANTORO, F., PETRONGOLO, C., and LAM, A., 2000, *J. chem. Phys.*, **113**, 4073.
[70] DUNN, T. J., SWEETSER, J. N., WALMSLEY, I. A., and RADZEWICZ, C., 1993, *Phys. Rev. Lett.*, **70**, 3388.
[71] ASSION, A., BAUMERT, T., GEISLER, M., SEYFRIED, V., and GERBER, G., 1998, *Eur. Phys. J.* D, **4**, 145.
[72] STAPELFELD, H., CONSTANT, E., and CORKUM, P. B., 1995, *Phys. Rev. Lett.*, **74**, 3780.
[73] CHELKOWSKI, S., CORKUM, P. B., and BANDRAUK, A. D., 1999, *Phys. Rev. Lett.*, **82**, 3416.
[74] SEEL, M., and DOMCKE, W., 1991, *Chem. Phys.*, **151**, 59.
[75] SEEL, M., and DOMCKE, W., 1991, *J. chem. Phys.*, **95**, 7806.
[76] MEIER, C., and ENGEL, V., 1993, *Chem. Phys. Lett.*, **212**, 691.
[77] MEIER, C., and ENGEL, V., 1994, *J. chem. Phys.*, **101**, 2673.
[78] BRAUN, M., MEIER, C., and ENGEL, V., 1996, *J. chem. Phys.*, **105**, 530.
[79] BRAUN, M., and ENGEL, V., 1997, *Z. Phys.* D, **39**, 301.
[80] ARASAKI, Y., TAKATSUKA, K., WANG, K., and MCKOY, V., 1999, *Chem. Phys. Lett.*, **302**, 363.
[81] ARASAKI, Y., TAKATSUKA, K., WANG, K., and MCKOY, V., 2000, *J. chem. Phys.*, **112**, 8871.

[82] CYR, D. R., and HAYDEN, C. C., 1996, *J. chem. Phys.*, **104**, 771.
[83] GREENBLATT, B. J., ZANNI, M. T., and NEUMARK, D. M., 1996, *Chem. Phys. Lett.*, **258**, 523.
[84] BLANCHET, V., and STOLOW, A., 1998, *J. chem. Phys.*, **104**, 771.
[85] STERT, V., RADLOFF, W., SCHULZ, C. P., and HERTEL, I. V., 1999, *Euro. Phys. J.* D, **5**, 97.
[86] DAVIES, J. A., LECLAIRE, J. E., CONTINETTI, R. E., and HAYDEN, C. C., 1999, *J. chem. Phys.*, **111**, 1.
[87] FARMANARA, P., RADLOFF, W., STERT, V., RITZE, H.-H., and HERTEL, I. V., 1999, *J. chem. Phys.*, **111**, 633.
[88] BLANCHET, V., ZGIERSKI, M. Z., SEIDEMAN, T., and STOLOW, A., 1999, *Nature*, **401**, 52.
[89] FROHNMEYER, T., HOFMANN, M., STREHLE, M., and BAUMERT, T., 1999, *Chem. Phys. Lett.*, **312**, 447.
[90] FROHNMEYER, T., and BAUMERT, T., 2000, *Appl. Phys.* B, **71**, 259.
[91] ASSION, A., GEISLER, M., HELBING, J., SEYFRIED, V., and BAUMERT, T., 1996, *Phys. Rev.* A, **54**, R4605.
[92] ASSION, A., BAUMERT, T., SEYFRIED, V., WEISS, V., WIEDENMANN, E., and GERBER, G., 1996, *Z. Phys.* D, **36**, 265.
[93] MEIER, C., and ENGEL, V., 1996, *The Reaction Path: Concepts and Methods*, edited by D. Heidrich (Dordrecht: Kluwer), p. 283.
[94] FARMANARA, P., STEINKELLNER, O., WICK, M. T., WITTMANN, M., KORN, G., STERT, V., and RADLOFF, W., 1999, *J. chem. Phys.*, **111**, 6264.
[95] ENGEL, V., and HENRIKSEN, N. E., 2000, *J. chem. Phys.*, **112**, 106.
[96] SAKURAI, J. J., 1985, *Modern Quantum Mechanics* (Redwood City, California: Addison-Wesley).
[97] LEONARD, U., and RAYMER, M. G., 1995, *Phys. Rev. Lett.*, **76**, 1985.
[98] CHEN, X., and YEAZELL, J. A., 1997, *Phys. Rev. Lett.*, **56**, 2316.
[99] LEICHTLE, C., SCHLEICH, W. P., AVERBUKH, I. SH., and SHAPIRO, M., 1998, *Phys. Rev. Lett.*, **80**, 1418.
[100] SCHLEICH, W. P., and RAYMER, M. (editors), 1997, *J. mod. Optics*, **44**.
[101] DUNN, T. J., WALMSLEY, I. A., and MUKAMEL, S., 1995, *Phys. Rev. Lett.*, **74**, 884.
[102] WINACHT, T. C., AHN, J., and BUCKSBAUM, P. H., 1998, *Phys. Rev. Lett.*, **80**, 5508.
[103] PAULI, W., 1933, *Handb. Phys.*, **24**.
[104] GERCHBERG, R. W., and SAXTON, W. O., 1972, *Optik*, **34**, 227.
[105] SCHISKE, P., 1973, *Optik*, **40**, 261.
[106] HUISER, A. M. J., DRENTH, A. J. J., and FERWERDA, H. A., 1976, *Optik*, **45**, 303.
[107] YANG, G., DONG, B., GU, B., ZHUANG, J., and ERSOY, O. K., 1994, *Appl. Optics*, **33**, 209.
[108] LEIN, M., ERDMANN, M., and ENGEL, V., 2000, *J. chem. Phys.*, **113**, 3609.
[109] HENRIKSEN, N. E., 1998, *Comments atom. molec. Phys.*, **21**, 153.
[110] TAYLOR, J. R., 1972, *Scattering Theory: The Quantum Theory on Nonrelativistic Collisions* (New York: Wiley).
[111] KOSLOFF, R., and BAER, R., 1991, *Mode Selective Chemistry*, edited by J. Jortner, R. D. Levine and B. Pullman (Dordrecht: Kluwer), p. 347.
[112] MEIER, C., and ENGEL, V., 1994, *Phys. Rev. Lett.*, **73**, 3207.